Nucleic Acids Research, 2025, **53**, gkaf146
https://doi.org/10.1093/nar/gkaf146
Gene regulation, Chromatin and Epigenetics

Genome-wide transcriptional silencing and mRNA stabilization allow the coordinated expression of the meiotic program in mice

Laura Bellutti[1,2,†], Edith Chan Sock Peng[3,†], Victoria Cluzet[1,2], Marie-Justine Guerquin[1,2], Antoine Rolland[3], Sébastien Messiaen[1,2], Elena Llano[4], Ihsan Dereli[5], Emmanuelle Martini[1,2], Attila Tóth[5], Alberto M. Pendás[4], Frederic Chalmel[3,*], Gabriel Livera[1,2,*]

[1]Université Paris Cité, CEA, Genetic Stability Stem Cells and Radiation, Laboratory of Development of the Gonads, F-92265 Fontenay-aux-Roses, France
[2]Université Paris-Saclay, CEA, Genetic Stability Stem Cells and Radiation, LDG/IRCM/IBFJ, F-92265 Fontenay-aux-Roses, France
[3]Inserm, EHESP, Univ Rennes, Irset (Institut de recherche en santé, environnement et travail)—UMR_S 1085, Rennes, France
[4]Molecular Mechanism Program, Centro de Investigation del Cancer (Universidad de Salamanca-CSIC), 37007 Salamanca, Spain
[5]Institute of Physiological Chemistry, Faculty of Medicine at the TU Dresden, Fiedlerstrasse 42 01307 Dresden, Germany

[*]To whom correspondence should be addressed. Email: gabriel.livera@cea.fr
Correspondence may also be addressed to Frederic Chalmel. Email: frederic.chalmel@inserm.fr
[†]The first two authors should be regarded as Joint First Authors.

Abstract

The transcriptional dynamic of mammalian cells when these transit from the ubiquitous mitotic to a meiotic-specific program is key to understand this switch central to sexual reproduction. By quantifying active RNA polymerase II and nascent transcripts using single cell dataset and ethynyl-uridine pool-down with sorted cells from synchronized testes, we detailed the transcriptional activity of murine male germ cells. When spermatogonia differentiate, transcription slows down, reaching minimal activity at meiotic entry and resumes during pachytene stage. This event, we termed EMLT (for early meiotic low transcription), is distinct from the silencing of sex chromosomes as it is independent of Setdb1, though it is accompanied by the same chromatin mark, H3K9me3. EMLT is delayed in Stra8KO but occurs in mutants altering meiotic chromosome structure or double-strand break formation or repair. By comparing transcript abundance and nascent transcription we unveil a massive event of messenger RNA stabilization that parallels EMLT. Altogether our data indicate that meiosis is initiated with a nearly silent genome, and we propose that the stabilization of transcripts at that time facilitates the meiotic entry by synchronizing the expression of several meiotic subprograms.

Graphical abstract

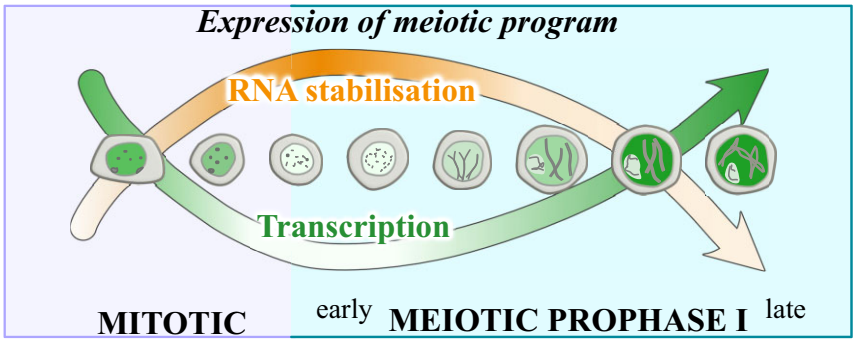

Introduction

Spermatogenesis relies on specific and complex transcriptional programs to orchestrate the production of male gametes [1]. It can be divided into a mitotic phase, a meiotic phase, and a post-meiotic phase. Spermatogonial stem cells multiply and enter a differentiation pathway. In the mouse, this leads to a strictly regulated differentiation of type A spermatogonia into type A1–A4, intermediate, and B spermatogonia through successive cell divisions [2]. Type B spermatogonia are the precursors of preleptotene cells entering the premeiotic S phase.

Received: May 5, 2024. **Revised:** February 6, 2025. **Editorial Decision:** February 9, 2025. **Accepted:** March 13, 2025

The spermatocytes undergo two consecutive meiotic divisions allowing the production of haploid spermatids [3]. Finally, the process termed spermiogenesis includes several morphological transformations of spermatids generating the highly differentiated spermatozoa [4]. Each step of spermatogenesis requires the regulated and dynamic expression of specific transcripts, contributing to the high diversity of testicular transcriptome [5–7]. Additionally, several transcriptional arrests and post-transcriptional regulations complicate the testicular transcriptome [8]. Two transcriptional arrests have been exquisitely characterized: the silencing of sex chromosomes during meiosis, a process termed meiotic sex chromosome inactivation (MSCI) and a global silencing in post-meiotic elongated spermatids undergoing tight packaging of the genetic material [9].

A critical step of spermatogenesis consists in the conversion of mitotic spermatogonia into meiotic spermatocytes. Stimulated from retinoic acid 8 (STRA8) is a transcription factor mandatory to orchestrate the mitosis-to-meiosis transition [10]. Meiosis begins with a long prophase I that is subdivided into different stages: leptotene, zygotene, pachytene, and diplotene. During prophase I, programmed DNA double-strand breaks (DSBs) are generated at specific regions called 'hotspots' [11, 12]. DSBs are next repaired by meiotic homologous recombination (HR). In parallel, homologous chromosomes align, pair, and synapse thanks to the formation of a proteinaceous structure called the synaptonemal complex (SC). At the end of pachytene stage, DSBs are repaired and autosomes are fully synapsed. In contrast, X and Y chromosomes remain largely unsynapsed because of their lack of homology. They are compartmentalized in a heterochromatic structure called sex body. The sex body is transcriptionally inactive due to DNA damage response and chromatin regulation that induce the MSCI [9, 13–16].

DSBs generation, HR and SC formation are highly regulated and interdependent processes. The expression of meiotic-specific genes allows fine regulation of these events. Indeed, meiotic initiation is characterized by an extensive genome reprogramming, to switch from a mitotic program to a meiotic one. This is accompanied by elaborated post-transcriptional mechanisms changing messenger RNA (mRNA) stability and alternative splicing events [8, 17]. The mechanisms governing such considerable changes in the transcriptome are yet poorly understood and may be connected to the major events occurring in the meiotic genome. Interestingly, spermatocytes in the early stages of prophase I have been reported with a very low or near-extinct transcriptional activity [18–20]. This genome-wide low transcription level, together with the existence of specific meiotic transcripts and transcriptional regulations, is puzzling. Currently, very little is known about this global transcriptional reduction, contrarily to MSCI, which is largely characterized. Few transcriptome analyses have focused on spermatocytes initiating meiotic prophase I, due to the difficulty in isolating these rare testicular cell populations. Moreover, transcriptome analyses poorly reflect transcription, as these are in part blurred by post-transcriptional mechanisms.

Here, we characterized the global reduction of transcriptional activity in the genome of early meiotic cells. In order to acquire a precise view of transcription dynamic around meiotic entry, we employed spermatogenesis synchronization, cell sorting, and ethynyl uridine incorporation to specifically label nascent RNAs, comparing this with unspliced RNA analysis via scRNA-seq. We demonstrated that this decrease of transcription precedes and is independent of the key events of prophase I, DSBs, and chromosome synapsis, but depends on the meiotic gatekeeper *Stra8*. Interestingly, this low transcriptional activity is accompanied by a broad stabilization of mRNA at the time of meiotic engagement.

Materials and methods

Mice and animals

All animal studies were conducted in accordance with the guidelines for the care and use of laboratory animals of the French Ministry of Agriculture (France, APAFIS#32392-2021071211498973). Mice were housed in controlled photoperiod conditions (lights on from 08:00 to 20:00) and supplied with commercial food and tap water ad libitum. Synchronization of spermatogenesis in NMRI mice was performed as previously described [21]. Two milligram of five-ethynyl uridine (EU, Click-iT™ Nascent RNA Capture Kit, Invitrogen) per mouse were injected at 24 days post-partum (dpp) to label nascent RNA. Three hours later, mice were sacrificed and cells were FACS-sorted based on their ploidy to isolate spermatogonia, leptotene, and pachytene spermatocytes as previously described [22, 23]. Cells from two to four animals were pooled together for RNA extraction and nascent RNA capture, representing over 700 000 cells per point. For each cell population, experiments were run in triplicate (i.e. three independent RNA pools for spermatogonia, leptotene, and pachytene cells). Cells obtained through the spermatogenesis synchronization protocol were used exclusively for EU-RNA-seq. All the other experiments were performed on animals without synchronization.

To study ovary development, timed matings were set up by housing males with females overnight. The presence of a vaginal plug was checked the following morning. The following midday was designated as 0.5 days post-conception (dpc). Pregnant females were sacrificed by cervical dislocation, fetuses were removed from uterine horns, and gonads were dissected under a binocular microscope.

All transgenic mice used in this study have been previously described [13, 17, 23–29]. Gonads from dogs, cats, and goats were obtained following castrations performed in veterinary clinics. All procedures involving non-murine species adhered to ethical standards set by veterinary practices.

Preparation of spermatocyte chromosome spreads

Testes used for spermatocyte spread preparations were collected from adult mice (2–6 months). For wild type (WT), *Spo11*$^{-/-}$, *Meiob*$^{-/-}$, *Setdb1*$^{-/-}$, and *Atr*$^{fl/-}$; *Atm*$^{-/-}$ mice, spermatocyte spreads were prepared as follows. Spermatocytes were manually liberated from tubules (flat razor blades) and resuspended in 0.1M sucrose. Ovaries used for chromosome spreads were collected from 14.5 dpc embryos, 18.5 dpc embryos, and 0 dpp pups. Ovaries were dilacerated in 0.1M sucrose on slides using needles. Oocytes or spermatocytes were then distributed on slides in humid chambers and fixed with 1% PFA (in H2O, pH 9.2) and 0.1% Triton for 1 h 30 min. After fixation, slides were rinsed with H2O 0.4% Photo-Flo 200 (Kodak).

Immunofluorescence on meiocyte chromosome spreads

After washing chromosome spreads from spermatocytes or oocytes, slides were air-dried before blocking. Slides were incubated for 1 h at room temperature with blocking solu-

tion (0.2% BSA, 0.2% Gelatin, 0.05% Tween in PBS) and overnight with primary antibodies in blocking solution at room temperature (see Table S1 for antibodies). Secondary antibodies were incubated for 1 h 30 min at 37°C. Slides were stained with 4′,6-diamidino-2-phenylindole (DAPI) and mounted with Prolongold medium. Imaging was performed using a Leica DM5500 B epifluorescence microscope (Leica Microsystems) equipped with a CoolSNAP HQ2camera (Photometrics) and Leica MMAF software (Metamorph, Molecular Devices). Images were processed with ImageJ software.

Immunohistostaining

Gonads were fixed in 4% PFA, dehydrated, embedded in paraffin, and cut into 5-µm-thick sections. Sections were mounted on slides, dewaxed, rehydrated, and boiled for 20 min in citrate buffer (pH 6) prior to immunostaining. For immunofluorescence stainings, sections were blocked for 1h in Gelatin blocking solution (0.2% BSA, 0.2% Gelatin, 0.05% Tween in PBS) and incubated 1 h 30 min at 37°C with the primary antibody diluted in blocking solution (see Table S1 for antibodies). After three washes in PBS 0.05% Tween, slides were incubated with secondary antibodies for 1 h at 37°C. Slides were treated with DAPI and mounted in ProLong Gold. Imaging was performed using a spinning-disk confocal microscope (Nikon Ti2, CSU-W1) with Metamorph software. Images were processed with ImageJ software.

RNA polymerase II quantification

For all experimental comparisons, exposure time and laser intensity settings were kept constant, and saturation was avoided during image acquisition. Quantitative analyses were performed on unsaturated raw images, and representative images were adjusted to highlight faint signals while maintaining uniform settings within each panel. Quantification of RNA polymerase II, total (POL2) or phosphorylated (pPOL2), on chromosome spreads was performed with ImageJ software. DAPI staining was used to delimit nuclei of cells, and the mean intensity of POL2 was quantified within these regions. Background intensity was subtracted from the nuclear signal to ensure accurate measurements.

Fluorescence intensity of POL2 and pPOL2 on testes sections was quantified with ImageJ software using line scans on a single focal plane (plot profile). DAPI staining was employed to identify nuclear boundaries and used to draw a line crossing the nucleus of the cell. We termed this line 'cell diameter'. Background noise for POL2 and pPOL2 was measured using a line scan of similar length outside the cell nucleus. Values of the background line scan were averaged, and for each section across the line scan, the intensity level of POL2 and pPOL2 was normalized to the mean background intensity. For POL2 and pPOL2 comparisons, quantifications were performed on the same cells.

RNA-sequencing data analysis

For EU-RNA-seq, capture of nascent RNA was performed according to the manufacturer instructions (Click-iT™ Nascent RNA Capture kit, Invitrogen). RNA-seq libraries were generated using Next Ultra II Directional RNA Library Prep kit (NEB) and ribosomal RNA depletion according to the manufacturer's protocols. EU-RNA-seq libraries were made like the RNA-seq but without any depletion. Libraries were sequenced on an Illumina HiSeq2500 aiming at an average of 60 million 100-bp reads per sample. Raw reads from the EU-RNA-seq and RNA-seq datasets were mapped onto the mouse genome (mm10) by using STAR (v2.5.2a). The *StringTie* tool was used for transcript assembly while Ballgown was used for quantification to get a FPKM expression matrix. After quantification, the resulting FPKM expression matrix from the EU-RNA-seq dataset was corrected according to the expression of 5S ribosomal genes, which are considered transcriptionally stable during spermatogenesis. The expression matrix was divided by the weighted sum of all 5S ribosomal genes.

Single-cell RNA-sequencing data analysis

Pre-processing and quality control

Mouse scRNA-seq data were downloaded from the EBI (E-MTAB-6946) [20]. These included 10 samples from mice aged 5–42 dpp. Raw sequencing reads were processed and mapped to the mouse (mm10) genomes using *CellRanger* (v4) with default parameters, and all samples were aggregated with cellranger aggr. Outlier cells were removed from the aggregated matrices with *Scater* [30]. In parallel, *DoubletFinder* [31] was used for doublet detection and removal on each individual sample. Finally, *Scater* and *Scran* [32] were used to exclude genes detected in <10 cells.

The *Seurat* (v3) analysis pipeline [33] was then applied. Data normalization was performed with the LogNormalize function with default parameters, while the 2000 most variable genes were identified with FindVariableFeatures. A linear dimensionality reduction was then performed with RunPCA and a JackStraw procedure was used to identify the number of dimensions to be considered. The FindNeighbors and FindClusters functions were applied to determine cell clusters. Correction of batch effects was performed using the Seurat's CCA method. Data visualization was finally achieved using the uniform manifold approximation projection (UMAP) dimensional reduction technique applied to the batch effect corrected data. Following identification of main cell populations based on known marker genes, germ cell clusters were subsetted and submitted using the same pipeline as described above, i.e. applying FindVariableFeatures, RunPCA, JackStraw, FindNeighbors, FindClusters, and CellCycleScoring. Again, the clusters were annotated based on known marker genes and the resulting annotation was validated by comparison to that of Ernst and collaborators using the hypergeometric statistical test as well as by monitoring germ cell evolution according to sample ages and cell cycle phase.

Quantification of nascent transcription and correction of ploidy effect

Next the velocyto tool was used [34] to generate unspliced and spliced count data starting from bam files from Cell Ranger, to quantify nascent transcription and transcription, respectively. Unspliced scRNA-seq data were used as a proxy for nascent transcription measurement in order to study transcriptional activity during spermatogenesis. The number of unspliced counts for each cell was calculated independently for autosomes and sex chromosomes. Since the amount of DNA by cell can directly influence the number of RNA molecules that are produced in each cell, the DNA content of each germ cell subpopulation was taken into account: for undifferentiated and differentiating spermatogonia (2n/2c) and for secondary spermatocytes (1n/2c), the number of unspliced counts was unchanged; for primary spermatocytes (leptotene, zygotene,

pachytene, diplotene, and metaphase I; 2n/4c), the number of unspliced counts were divided by two; while for spermatids (1n/1c), the number of unspliced counts was multiplied by two.

Identification of escaping and silenced genes during EMLT

Since ploidy-corrected unspliced count matrix was employed, intron size may bias the number of quantified reads per gene. To avoid this effect, a cumulative intron size correction was applied. For each gene: (i) intron size was obtained by subtracting the cumulative sum of exons using the Bedtools subtractBed function, (ii) this value was then used to divide gene count and the ratio was multiplied by an arbitrary constant (1 000 000). This normalization allows setting of a threshold for expressed gene detection. Genes showing a null variance were discarded. Next, a two-step process was used to identify potential 'silenced' and 'escaping' genes. Genes were considered 'silenced' if their expression values were: (i) higher than an expression threshold (median value of the overall count matrix = 0.07) in at least one of the relevant stages (Diff Spg 1, Diff Spg 2, ePa 1, ePa 2, lPa, and/or Di) and, (ii) significantly correlated (one-tailed Pearson correlation test, P -value <.05) to the expression profiles of archetypal genes (*Ndufa11* and *Park7*) showing a silenced expression pattern in Le and Zy. Genes were considered 'escaping' if their expression values were: (i) >0.07 in Le and Zy and (ii) significantly correlated (*P-value* <.05) to archetypal genes (*Pet2*, *Ccnb3*, and *Prdm9*) showing an escaping expression pattern in Le or Zy. The median value of the overall count matrix was chosen as the expression threshold because it provides a robust and data-driven criterion for filtering extreme values while ensuring reproducibility across datasets.

RNA stability

RNA stability during meiosis was investigated using both single-cell and bulk RNA-seq approaches. For the scRNA-seq dataset the 'spliced' and 'unspliced' expression profiles reflect transcription and nascent transcription, respectively, while the 'stability' is the ratio of 'spliced' to 'unspliced' expression levels. In the RNA-seq dataset 'RNA-seq' and 'EU-RNA-seq' expression profiles reflect transcription and nascent transcription, respectively, while 'stability' is the ratio of 'RNA-seq' to 'EU-RNA-seq' expression levels.

Data representation: heatmaps and boxplots

Heatmaps and boxplots were generated using *Ggplot2* (R-package). For heatmaps expression values of each gene were scaled between [0;1] using a 0-max scale (0 = 0; maximum value = 1). Thanks to this scaling, zero can be regarded as an actual zero. Stability matrix was scaled between [0;1] with the Rescale () function from the *Scales* package.

Integration of gene expression with recombination hotspots and epigenetic marks

Data on DSB hotspots as defined by anti-DMC1 single-stranded DNA (ssDNA) sequencing data in C57BL/6J mice were downloaded from GEO (GSE75419) [35]. The distance of genes to the nearest hotspot out of 19 528 recombination sites was computed with the closest function from *BedTools* [36]. Two-tailed Wilcoxon tests were used to compare the distance to the nearest hotspot for 'silenced' genes or 1000 random intergenic regions. A DSB map defined by SPO11-oligonucleotides was also used to compare recombination sites to transcriptional changes [12].

ChIP-seq data for seven histone marks (H3K4me3, H3K4me1, H3K9me2, H3K9me3, H3K27me3, H3K36me3, and H3K27ac) obtained in spermatogenic cells were download from GEO (GSE132446) [37]. In this study histone modifications in homogenous synchronous spermatogenic cells of 9 or 10 spermatogenic stages (undifferentiated spermatogonia, type A1 spermatogonia, type B spermatogonia, mid-preleptotene spermatocytes, leptotene spermatocytes, mid-zygotene spermatocytes, early-pachytene spermatocytes, mid-pachytene spermatocytes, and diplotene spermatocytes) were studied. *DeepTools* was used to perform histone modification distribution analysis around 'silenced', 'escaping' genes and random intergenic regions. To focus on the events around the transcription start site (TSS), different upstream and downstream distances were used: −2000/+2000 pb for H3K9me3, H3K9me2, H3K27me3, and H3K4me1; −1000/+1000 for H3K27ac and H3K4me3; and 0/+2000 for H3K36me3. The histone modification scores associated with genomic regions of interest ('escaped', 'silenced' genes and random intergenic regions) were generated by *ComputeMatrix* modules. Bins for each cell type per genomic region were summed in the output matrix. Then profiles of histone modification scores for 'silenced', 'escaping' genes and random intergenic regions were represented using mean ± sem.

Results

Transcriptional quiescence initiates prior meiotic entry

To finely characterize transcriptional levels across spermatogenesis, we first quantified the active form of RNA polymerase II, phosphorylated on Serine 2 of its CTD (pPOL2), by immunofluorescence staining (Fig. 1A–G). Using spermatocyte chromosome spreads (Fig. 1A and B), pPOL2 was hardly detected on chromatin at leptotene and zygotene stages. By mid-pachytene stage, pPOL2 intensity rose sharply, peaking at late pachytene and diplotene stages, except on X and Y chromosomes, where it remained undetectable (Fig. 1A and Supplementary Fig. S1). Quantification in leptotene cells and in the sex body from mid-pachytene cells indicated an equivalent lack of transcriptional activity. This confirms and extends previous observations [9, 19]. We termed this process of genome-wide pPOL2 reduction during the beginning of prophase I, early meiotic low transcription (EMLT), to distinguish it from the MSCI process, which silences exclusively the sex chromosomes in later stages (i.e. pachynema and diplonema).

Next, we exploited the well-characterized seminiferous epithelium cycle to determine when EMLT initiates and ends during spermatogenesis. Measure of pPOL2 on testis sections show that type A spermatogonia displayed pPOL2 staining (Fig. 1C and D, and Supplementary Fig. S2), which decreased in intermediate and type B spermatogonia, and further diminished in preleptotene and leptotene spermatocytes. During zygonema, the staining increased slightly and progressively to reach at the early pachytene stage an intensity level similar to type A spermatogonia. Intensity of pPOL2 staining peaked at late prophase I and in first round spermatid stages. As expected, elongated spermatids were completely silenced and devoid of pPOL2 staining due to their high level of DNA

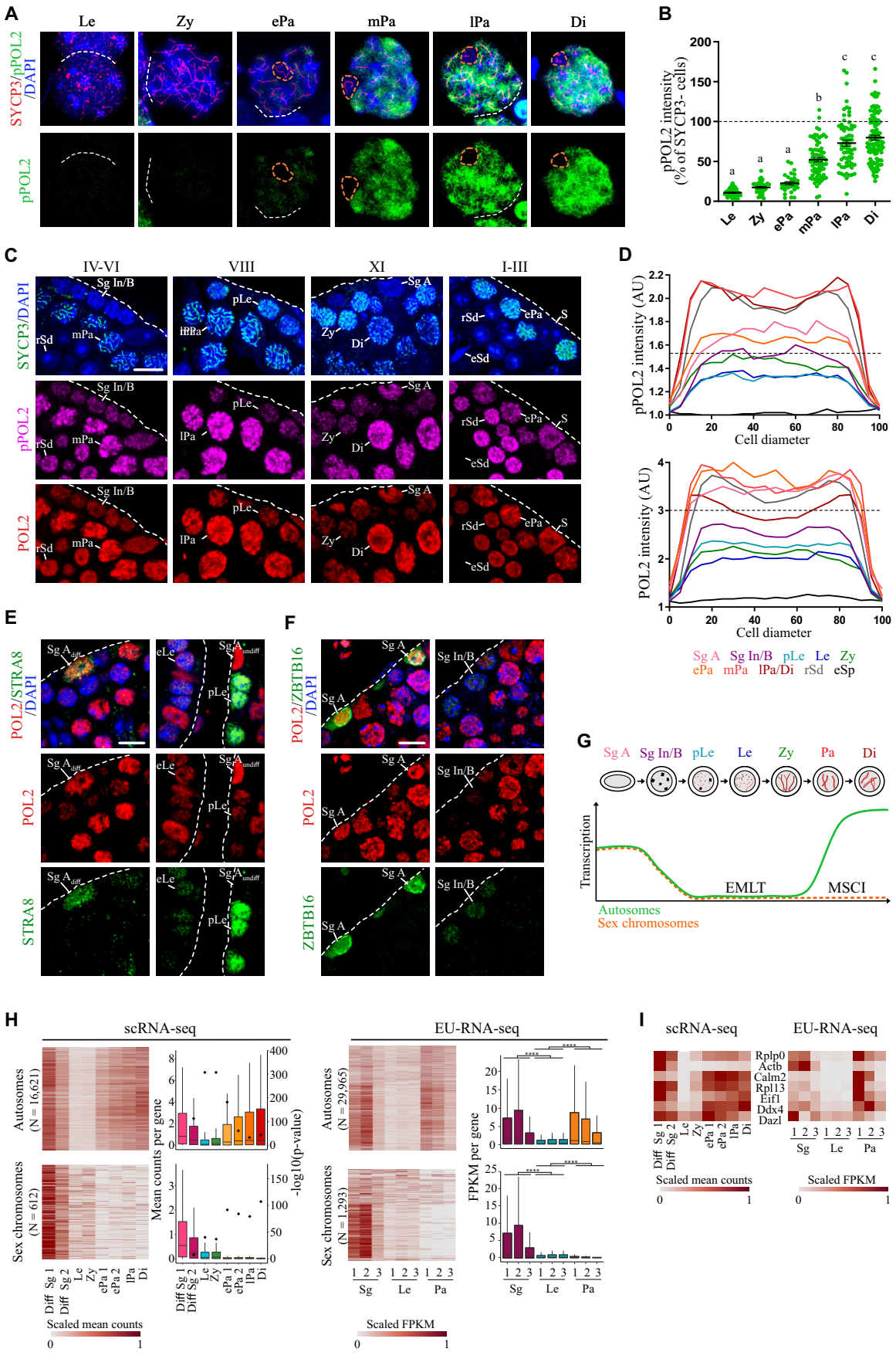

Figure 1. Dynamic of transcription during spermatogenesis. Characterization of RNA polymerase II phosphorylated on Serine 2 (pPOL2) profile during prophase I by co-immunolabelling of pPOL2 and SYCP3 on spermatocytes chromosome spreads (**A**). DNA is stained with DAPI. pPOL2 staining is very

compaction. Total RNA polymerase II (POL2), including non-phosphorylated and phosphorylated forms, had an expression profile similar to that of pPOL2 (Fig. 1C and D, and Supplementary Figs S1 and S2). Using chromosome spreads, we evidenced that POL2 was also hardly detected on the chromatin during EMLT (Supplementary Fig. S1). This indicates that the variations of pPOL2 intensity are due to a reduction in RNA polymerase II availability and/or loading on chromatin. Interestingly, early pachytene spermatocytes showed maximal POL2 levels, whereas pPOL2 reached its peak later, during mid-pachynema (Fig. 1D, and Supplementary Figs S2B and S3), suggesting a two-step process: first, the loading of POL2 onto chromatin, and second, the activation of POL2 (pPOL2) to produce the hyper-transcriptional state observed in late prophase I. Of note, after MSCI initiated, POL2 but not pPOL2 reappeared specifically on the axes of sex chromosomes (Supplementary Fig. S1A), while during EMLT both were absent from the whole chromatin.

To determine accurately when EMLT was set up during spermatogonia differentiation, we monitored two spermatogonia markers: STRA8 and ZBTB16 (Fig. 1E and F). Undifferentiated spermatogonia, that expressed ZBTB16 but not STRA8, and differentiating type A spermatogonia, that expressed ZBTB16 and STRA8 at low level, were stained for POL2. Intermediate and type B spermatogonia, in which ZBTB16 was weakly detected ([38] and personal observations), were faintly stained for POL2. Thus, EMLT initiates during spermatogonia mitotic divisions, more precisely at the transition from type A spermatogonia to intermediate spermatogonia (Fig. 1G).

To obtain a measure of transcription, we first analysed published dataset from single cells (scRNA-seq). The study of Ernst *et al.* did not discard droplets containing very few RNAs and was thus well suited to analyse cells with a low transcription [20]. Data were downloaded from the EBI database and visualized with UMAP to identify germ cell stages. Thirty-four thousand seventy-eight germ cells were selected and partitioned into 30 clusters (Supplementary Figs S4, S5, and S6). We then analysed unspliced RNAs as a proxy to monitor nascent transcription. Ploidy effect was corrected as a function of the spermatogenic stage as transcription is strongly associated to ploidy. Gene with null variance were removed, and scaled expression of the 17 233 remaining genes was visualized as a heatmap according to their chromosomal location (autosomes and sex chromosomes). This approach validated the two well-known transcriptional arrests during spermatogenesis, the MSCI during the pachytene stage and the global inactivation during spermiogenesis (Supplementary Fig. S6C). Global silencing was observed at the leptotene and zygotene stages (Fig. 1H and Supplementary Fig. S6C). Total nascent transcription decreased 12-fold between spermatogonia (Diff Sg1) and leptonema.

Second, we directly captured nascent transcripts using ethynyl-uridine incorporation and sequencing (EU-RNA-seq). EU incorporation was performed in post-natal testes with synchronized spermatogenesis and spermatogonia, leptotene and pachytene cells were sorted simultaneously (Supplementary Fig. S7A). This approach allowed minimizing contaminations and enrichment of rare stages. Given the fact that EU-RNA-seq relies on artificially synchronized spermatogenesis we ensure that EMLT takes place similarly (Supplementary Fig. S7B) and carefully compare data obtained from this approach with scRNA-seq performed in non-synchronized animals. EU-RNA-seq identified nascent RNA and also evidenced EMLT and MSCI at the leptotene and pachytene stages, respectively (Fig. 1H). EU-RNA-seq allowed the analysis of nearly twice as much genes (31 258) in comparison to scRNA-seq. Comparison of gene transcription with both approaches revealed similar profiles as exemplified by a set of robustly expressed genes (reference genes or germ cell markers, Fig. 1I).

Altogether, staining for pPOL2 and POL2, pre-mRNA analysis (unspliced scRNA-seq), and nascent RNA analysis (EU-RNA-seq) confirmed the existence of EMLT. This silencing is initiated prior to meiotic entry and is most pronounced at the leptotene stage in mouse testicular cells.

←

low at leptotene (Le), zygotene (Zy), and early-pachytene stages (ePa) and is obvious at mid-pachytene (mPa), late-pachytene (lPa), and diplotene (Di) stages. Sex body (orange dashed circle) is not stained for pPOL2. Quantification of pPOL2 staining (**B**). pPOL2 intensity is normalized to SYCP3-negative cells (SYCP3-, 100%, black dashed line). Each dot represents one spermatocyte. Spermatocytes were harvested from seven mice; black bars represent means ± sem. For each column, different letters indicate significantly different values [ordinary one-way analysis of variance (ANOVA), multiple comparisons]. Immunofluorescence analysis of pPOL2 and total RNA polymerase II (POL2) in testis sections (**C**). Roman numbers indicate the stage of seminiferous epithelium cycle. Prophase I cells are identified thanks to SYCP3 and DNA is stained with DAPI. For panels (A), (E), and (F), dotted white lines delimit seminiferous tubules. Scale bar = 5 μm. Quantification of pPOL2 (upper) or POL2 (lower) intensity at each stage of spermatogenesis by line plot analysis in the nuclei (**D**). Each line represents the average of several cells at a specific spermatogenic stage. Sg A = Type A spermatogonia, $n = 19$; Sg Int/B = intermediate and type B spermatogonia, $n = 26$; pLe = preleptotene, $n = 27$; Le = leptotene, $n = 27$; Zy = zygotene, $n = 22$; ePa = early pachytene, $n = 27$; mPa = mid pachytene, $n = 50$; lPa/Di = late pachytene/diplotene, $n = 32$; rSd = round spermatids, $n = 50$; and eSd = elongated spermatids, $n = 4$. Black dashed line represents pPOL2 intensity in Sertoli cells (S, $n = 28$). AU = arbitrary units. Immunofluorescence analysis of POL2 and STRA8 in testis sections (**E**). DNA is stained with DAPI. Differentiated A spermatogonia (Sg Adiff), pLe and early-leptotene (eLe) cells are stained for STRA8 and show different levels of POL2 intensity. Immunofluorescence analysis of POL2 and ZBTB16 in testis sections (**F**). DNA is stained with DAPI. Sg A and Sp Int/B are stained for ZBTB16 and show different levels of POL2 intensity. Schematic representation of EMLT during spermatogenesis, with a focus on meiotic prophase I (**G**). Transcription level decreases during spermatogonia differentiation to reach minimum at preleptotene and leptotene stages. Transcription is hyperactivated at mid-pachytene and diplotene stages when sex chromosomes remain silent (MSCI). Heatmaps and boxplots of the expression of 17 233 and 31 258 genes distributed according to their chromosomal location (autosomes and sex chromosomes) from the unspliced scRNA-seq dataset (average count matrix) and the EU-RNA-seq dataset (FPKM matrix), respectively (**H**). These datasets reflect nascent transcription, and are used to study transcriptional activity during spermatogenesis. In the heatmaps, each row represents a gene, and each column represents a specific spermatogenic cell population (scRNA-seq) or a sample (EU-RNA-seq). For heatmaps, expression values (mean counts or FPKM) of each gene were scaled between [0;1] using a 0-max scale (0 = 0; maximum value = 1). Boxplots display the mean counts per gene and the FPKM values for unspliced scRNA-seq and for EU-RNA-seq, respectively. One-tailed Wilcoxon tests were used to compare the average counts or FPKM of each spermatogenic stage to the first spermatogenic cells analysed; a second axis representing the −log10 (*P*-value) indicates the test significance for scRNA-seq; **** indicates $P < .0001$ for EU-RNA-seq. Diff Sg = differentiated spermatogonia. For EU-RNA-seq, 1, 2, and 3 correspond to three independent experiments. Heatmaps representing the gene expression profiles of a subset of emblematic genes robustly expressed in the unspliced scRNA-seq and EU-RNA-seq datasets (**I**).

EMLT is conserved in mammalian testes and is observed in female mice

Since this meiotic genome-wide transcription arrest has, apart from *Mus musculus*, only been reported in males of a few species [39, 40], we sought to investigate its conservation in mammals. Interestingly, pPOL2 was almost undetectable at the beginning of prophase I in three different mammals: goat, rabbit, and dog (Supplementary Fig. S8A). As in mice, EMLT was also followed by a hyperactive transcriptional state in pachynema in these mammals. Altogether, this reflects a conserved dynamism of germ cells transcriptional state during spermatogenesis.

Meiosis occurs both during male and female gametogenesis. In females, meiosis begins during fetal life and arrests at the diplotene stage around birth. Transcriptional levels during prophase I have been poorly described in females. Thus, we analysed pPOL2 intensity in oocytes during prophase I (Supplementary Fig. S8B and C). We collected embryos at different fetal ages 14.5 and 18.5 days post-conception and at birth and performed chromosome spreads. pPOL2 staining was least abundant in leptotene and zygotene oocytes, lower than in somatic cells, and increased during late prophase I stages. However, there was a large heterogeneity in pPOL2 intensity in female meiocytes, whatever the stage, and many oocytes seem to escape a complete transcriptional repression. Thus, a process analogous to EMLT appears to also occur at meiotic entry in the female germline, albeit this phenomenon is less pronounced in the mouse developing ovary.

EMLT mechanism differs from MSCI

In order to search for epigenetic marks correlated to EMLT, we first partitioned genes in two opposite categories based on unspliced RNAs from scRNA-seq. 'Silenced' genes exhibited higher transcription levels both before and after EMLT, whereas 'escaping' genes were predominantly transcribed specifically during EMLT. Genes were identified by using a correlation-based analysis with archetypal genes, i.e. *Ndufa11* and *Park7* for the 'silenced' genes ($n = 11\ 660$), and *Pet2*, *Ccnb3*, and *Prdm9* for the 'escaping' genes ($n = 79$) (Fig. 2A and Supplementary Fig. S4B). We compared 'silenced' genes identified by scRNA-seq and EU-RNA-seq and all presented a low transcription in leptotene cells (Supplementary Fig. S9). As scRNA-seq presented a fine resolution of stages we next focus on silenced and escaping genes defined by this approach. More than 99% of 'silenced' genes were located on autosomes (11 590/11 660), whereas over 40% of 'escaping' genes (33/79) were found on sex chromosomes (32 on the X), and their profiles were roughly similar when assessed with EU-RNA-seq (Supplementary Fig. S10). Escaping genes are found scattered throughout the genome and are mostly protein coding genes (Table S2, Supplementary Fig. S11A). Most have a low expression in pachynema (including for escaping genes on autosomes) and are expressed again later in spermatids cells (Supplementary Fig. S11B).

We next analysed the profile of several histone marks associated with activation or repression of transcription using published ChIP-seq data [37] (Fig. 2B and Supplementary Fig. S12). None distinguished the 11 660 'silenced' from the 79 'escaping' genes. The histone H3K9me2 and me3 modifications around the TSS correlated with the timing of transcriptional quiescence. These marks are known to silence transcription. As H3K9me3 has been proposed to be involved in MSCI, we focused on this mark, it presented a gradual increase from undifferentiated spermatogonia to zygotene stages. This was confirmed by immunostaining in testicular sections (Fig. 2C). H3K9me3 staining was observed in patchy areas that likely correspond to pericentromeric heterochromatin. In the rest of the nucleus, staining was faint in A spermatogonia and pachytene spermatocytes and most abundant in leptotene and zygotene stages. As H3K9me3 has been proposed to repress transcription and is involved in MSCI, we sought to determine whether the same mechanisms govern MSCI and EMLT. During MSCI, sex chromosomes inactivation is primarily triggered by DNA damage response pathway and SETDB1 trimethylates H3K9 leading to the transient accumulation of H3K9me3 on sex chromosomes during early pachytene stages [13, 16, 19, 41]. We thus analysed pPOL2 in chromosome spreads from conditional KO obtained with the *Ngn3*-cre for *Setdb1* (*Setb1*$^{-/-}$) and for both *Atm* and *Atr* (*Atm*$^{fl/-}$; *Atr*$^{-/-}$). In these animals, MSCI has been reported greatly hampered at pachytene stage. At the leptotene stage, no pPOL2 was detected in the chromatin of both mutant mice indicating that impairment of key factors that govern MSCI do not alter EMLT (Fig. 2D). At the early pachytene stage, pPOL2 staining was retrieved in mutants as in WT animals indicating no defect in resuming transcription. To further compare MSCI and EMLT, expression profiles of 612 and 1293 genes located on the sex chromosomes were investigated in the unspliced scRNA-seq and the EU-RNA-seq datasets, respectively (Fig. 2E). scRNA-seq evidenced that nearly all genes investigated were extinct at the beginning of pachytene stage, many of which had transcriptional depression initiated before meiotic entry. In the EU-RNA-seq, three expression patterns were discernible. The first concerned genes silenced during EMLT but escaping MSCI, the second and predominant cluster was composed of genes silenced during both EMLT and MSCI, and the last cluster consisted of genes escaping EMLT but not MSCI (Fig. 2E, and c1, c2, and c3). Next, we focused on specific genes and gene families on sex chromosomes (Fig. 2F). The *androgen receptor* (*Ar*) gene was silenced both during EMLT and MSCI, a profile representative of most genes on sex chromosomes. Nascent RNAs of *Tex16*, *Dusp9*, and most genes of the *Mage* family were detected during EMLT, albeit possibly at lower levels than in spermatogonia, but not during MSCI. Genes from the Spin2 family on the contrary were specifically expressed during MSCI. Of note, Spin2 genes are mono-exonic and were thus discarded from the unspliced scRNA-seq data analysis. Altogether, these data indicate that MSCI is not just a mere extension of EMLT, as some genes on sex chromosomes display different expression dynamics and since key regulators of MSCI do not affect EMLT. Nonetheless repression of transcription may be associated in both cases with H3K9 methylation, possibly using different methylases.

EMLT is unaffected by cohesin or HORMAD1 depletion

At the beginning of prophase I, spermatocytes undergo specific chromatin rearrangements. Chromosomes form an axe/loop-structure. Sister chromatids are held together by cohesins allowing establishment of axial elements (AEs) at early leptotene [42]. To investigate the link between EMLT and chromosome structure, we analysed *Rad21L*$^{-/-}$ and *Stag3*$^{-/-}$ mice, which lack key meiotic-specific cohesins [27, 28, 42]. Mutation of these cohesins caused prophase I arrest at or

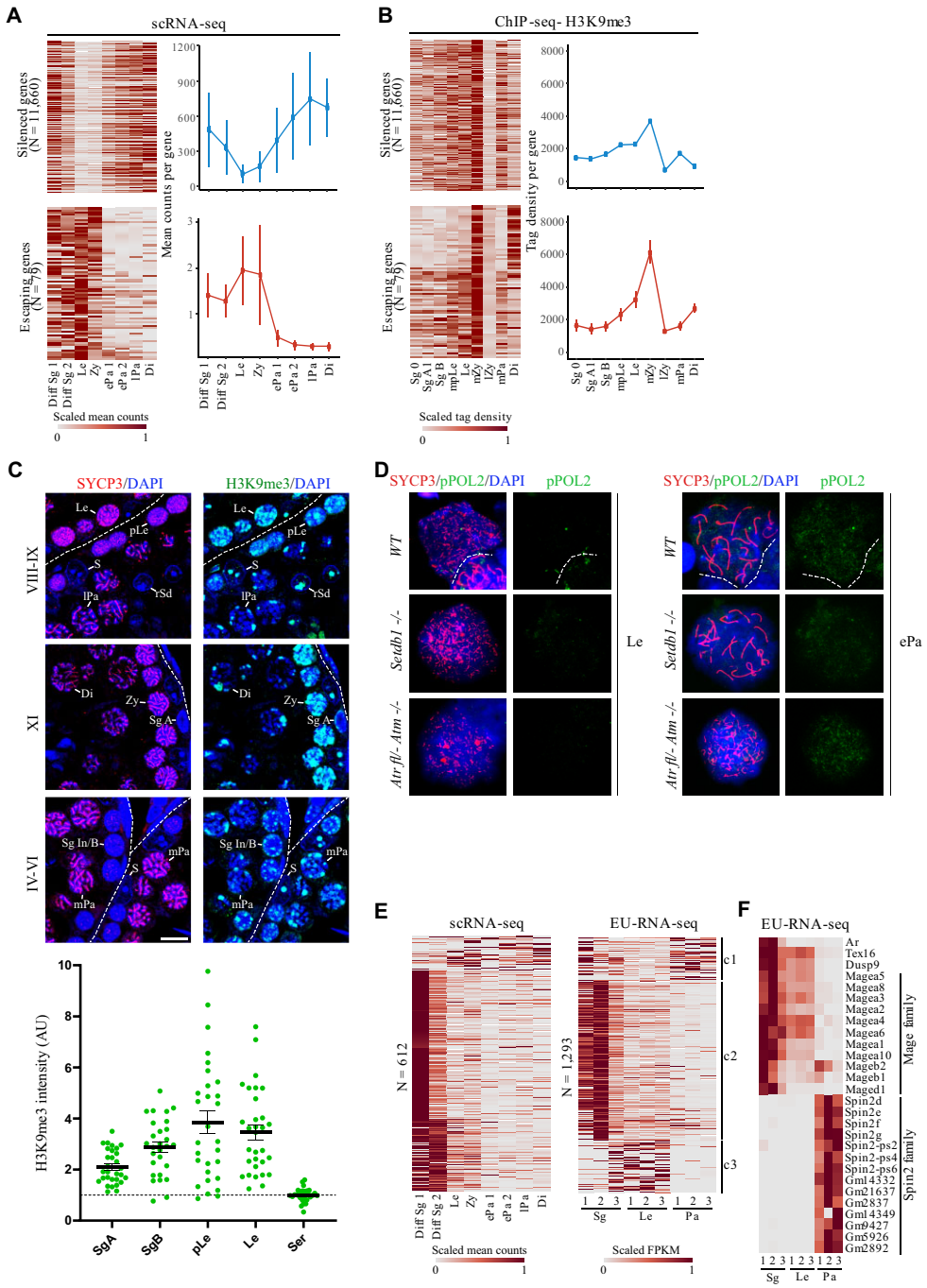

Figure 2. Gene expression profiles of 11 660 'silenced' and 79 'escaping' genes in the unspliced scRNA-seq dataset represented as heatmaps (scaled mean counts) and profile (mean counts per gene ± sem) (**A**). 'Silenced' and 'escaping' genes were identified by using a correlation-based analysis with archetypal genes. Quantification of the histone H3K9me3 modification around the TSS of the 11 660 'silenced' and 79 'escaping' genes according to ChIP-seq data from Chen *et al.*, (2020; GSE132446) (**B**). Heatmaps show the scaled tag density around the TSS from spermatogonia to diplotene spermatocytes: Sg 0 = undifferentiated spermatogonia; Sg A1 = type A1 spermatogonia; Sg B = type B spermatogonia; mpLe = mid-preleptotene spermatocytes; Le = leptotene spermatocytes; mZy = mid-zygotene spermatocytes; lZy = late zygotene spermatocytes; mPa = mid-pachytene spermatocytes; and Di = diplotene spermatocytes. The enrichment profiles of 'silenced' genes (blue) and 'escaping' genes (red) are represented using mean ± sem. Immunostaining for H3K9me3 and SYCP3 in testis sections from adult mice (**C**). DNA is stained with DAPI. Quantification of H3K9me3 intensity at each stage of spermatogenesis was performed (lower panel). Each line represents the average of several cells at a specific spermatogenic stage and the dashed line represents intensity in Sertoli cells (Ser). Legend is the same as in Fig. 1C. Co-labelling with SYCP3 and pPOL2 of spermatocyte chromosome spreads of WT, conditional KO mice for Setdb1 (*Setdb1*-/-), and conditional double KO for *Atr* and *Atm* (*Atr* fl/- *Atm* -/-) (**D**). Conditional inactivation of one *Setb1* and one *Atr* allele was mediated by *Ngn3*-cre (*Ngn3*-cre, *Setdb1* fl/- and *Ngn3*-cre, *Atr* fl/-, *Atm* -/-). All mice show weak pPOL2 staining at leptotene (Le) stage and an increase at early pachytene (ePa) stages. Heatmaps show the scaled expression profiles of genes located on the sex chromosomes in the unspliced scRNA-seq (scaled mean counts) and the EU-RNA-seq (scaled FPKM) datasets according to the scale bars (**E**). Clusters c1, c2, and c3 represent respectively genes escaping only MSCI, genes silenced during both EMLT and MSCI, and genes escaping EMLT but not MSCI. Heatmap representing the expression profiles of selected genes of interest for EMLT and for MSCI in the EU-RNA-seq (scaled FPKM) dataset (**F**). This dataset contains mono-exonic genes unlike the unspliced scRNA-seq dataset. The legends of heatmaps in panels (A), (E), and (F) are the same as for heatmaps in Fig. 1H.

before early pachynema. In both *Rad21L*$^{-/-}$ and *Stag3*$^{-/-}$, leptotene-like and zygotene-like spermatocytes displayed a low level of pPOL2, similar to that of WT mice (Fig. 3A and B). In *Rad21L* mutants, some spermatocytes resembling early pachytene stages presented a more intense staining for pPOL2 (Fig. 3B and C), albeit Rad21L mutation renders the staging of these cells uncertain.

Proper formation of AEs is mandatory to allow the synapsis of homologous chromosomes through completion of the SC. The HORMA domains protein HORMAD1 localises to unsynapsed chromosome axes and is removed soon after synapsis [26]. The disruption of *Hormad1* caused pairing defects and pachytene arrest. Leptotene and zygotene-like *Hormad1*$^{-/-}$ spermatocytes were faintly stained for pPOL2, with a quantified intensity similar to WT (Fig. 3A and B). Zygotene-like and early pachytene-like mutant spermatocytes appeared more robustly stained for pPOL2 that WT cells (Fig. 3C). However, the precise identification of these stages is uncertain in *Hormad1* mutants in which asynapsis signaling is defective. Of note, in WT early pachynema pPOL2 initially reappeared in highly localized areas emanating from the axes of the fully synapsed chromosomes (Supplementary Fig. S13). In *Hormad1*$^{-/-}$ spermatocytes, the reappearance of pPOL2 commenced on both synapsed and unsynapsed axes. This indicates that local synapsis is not a prerequisite for the reinitiation of transcription.

These results indicate that establishment of the meiotic-specific chromatin structure does not drive EMLT. In addition, completion of chromosome synapsis is not essential for concluding EMLT and transcriptional reactivation.

EMLT is independent of meiotic DSBs

As DSBs can be associated to transcriptional modifications in somatic cells, we speculated that in meiotic cells the formation of hundreds of DSBs might affect transcriptional activity. At the beginning of prophase I, DSBs are generated by the topoisomerase-like transesterase SPO11 at specific sites defined by the methyltransferase PRDM9 (PR/SET domain 9). DSBs are rapidly signaled by phosphorylation of H2AX (γH2AX) by the kinase ATM at leptotene stage. Interestingly, cells stained for γH2AX harbored low pPOL2 (Supplementary Fig. S14); this was obvious in early spermatocytes I and in intermediate and B spermatogonia that presented a weak but distinct γH2AX signal as previously reported [43]. To investigate if DSBs formation induces or maintains EMLT, we quantified pPOL2 in *Prdm9* and *Spo11* null spermatocytes (Fig. 4). In *Prdm9*$^{-/-}$ mice, DSBs are catalysed but do not localize correctly [25, 44, 45]. In *Spo11*$^{-/-}$ animals, programmed DSBs are not generated [46, 47]. In both cases, mutant spermatocytes arrest at zygotene/pachytene-like stage. Quantification of pPOL2 in section of *Prdm9*$^{-/-}$ testes revealed that EMLT was unchanged as hardly any staining was detected in leptotene and zygotene spermatocytes as in WT cells (Fig. 4A and B). This result is in accordance with EMLT being present in dog, which lacks *Prdm9* (Supplementary Fig. S8A). EMLT was also retrieved similarly in chromosome spreads from *Spo11*$^{-/-}$ spermatocytes (Fig. 4C and D). These data are consistent with a previous report [48]. Of note, in leptotene-like spermatocytes from *Spo11*$^{-/-}$ mice, pPOL2 intensity is slightly reduced compared to WT (Supplementary Fig. S15). This might indicate that in absence of DSB, transcription is even more repressed. Overall, we concluded that EMLT is not induced by programmed DSB.

Though *Prdm9*$^{-/-}$ and *Spo11*$^{-/-}$ mice are defective for DSBs localization and formation, respectively, in both mutants, γH2AX is still present, albeit at low level in *Spo11*$^{-/-}$ spermatocytes. We thus decided to analyse the transcriptional activity in *Atm* null mutants. We used *Atm*$^{-/-}$; *Spo11*$^{+/-}$ mice as these progress up to the diplotene stage allowing the study of transcriptional arrest (EMLT) and transcriptional reactivation. In these mutants, γH2AX signaling of DSBs occurring at leptotene stage is absent [49]. At leptotene and zygotene stages pPOL2 intensity was equivalent in WT and *Atm*$^{-/-}$; *Spo11*$^{+/-}$ spermatocytes (Fig. 4C and D). Reactivation of transcription at pachytene stage also occurs timely (Fig. 4E and F). This result indicates that DSB signaling does not influence EMLT.

In meiocytes, DSBs are rapidly repaired by HR and when global transcription is hyperactivated, few DSBs remain on autosomes from pachynemas. Meiosis specific with OB domains (MEIOB) is essential for completing meiotic recombination [23]. To assess the dependence of EMLT on HR, we analysed *Meiob* null mutants, which exhibit persistent DSBs. *Meiob*$^{-/-}$ spermatocytes showed a clear induction of EMLT, with minimal pPOL2 staining, similarly to WT leptonema and zygonema (Fig. 4C and D). In the absence of *Meiob,* prophase I arrested at early pachytene-like stage. The few mutant spermatocytes that reached this stage showed a mild elevation of pPOL2 signal, indicating that in the absence of DSB repair, transcription could be reactivated. Interestingly, pPOL2 reappeared as small patches in *Meiob*$^{-/-}$ spermatocytes and these localized both in synapsed and unsynapsed chromosomal domains (Supplementary Fig. S13B). This confirms the observation from *Hormad1* mutant revealing that synapsis is not required to terminate EMLT and to resume transcription.

Since DSBs do not appear to affect EMLT, we conjectured the reverse: that transcription might shape meiotic DSBs. Consequently, we thus tested the hypothesis that an association between recombination sites and transcriptional silencing may exist. To evaluate this hypothesis, the distance of the 'silenced' genes and 1000 random intergenic regions to the nearest recombination site was computed based on DSB hotspot data defined by anti-DMC1 ssDNA sequencing [35]. The distance distribution of the genes or regions to the nearest hotspots was plotted in a boxplot according to their chromosomal location (Fig. 4G). The 'silenced' genes were closer to the recombination sites than the random intergenic regions both on autosomes and sex chromosomes. These results suggest a possible link between distance to recombination sites and EMLT with DSBs occurring preferentially in transcriptionally silent domains. Nevertheless, given that both DSBs and silencing events occur throughout the whole genome, it was challenging to further test this relationship. Indeed, a detailed examination of a high-resolution DSB map provided by Spo11-oligonucleotides [12], revealed that distribution of DSBs and that of silenced genes largely overlapped. We exemplified this using chromosome 17 that contains several 'escaping' genes including the *Prdm9* (Fig. 4H). Albeit *Prdm9* is indeed located between two DSB hotspots, the presence of actively transcribed genes in leptotene is rare and is not systematic between distant hotspots.

Altogether these results indicate that EMLT is independent of the induction, signaling and repair of DSBs though it may be related to the localization of programmed DSBs.

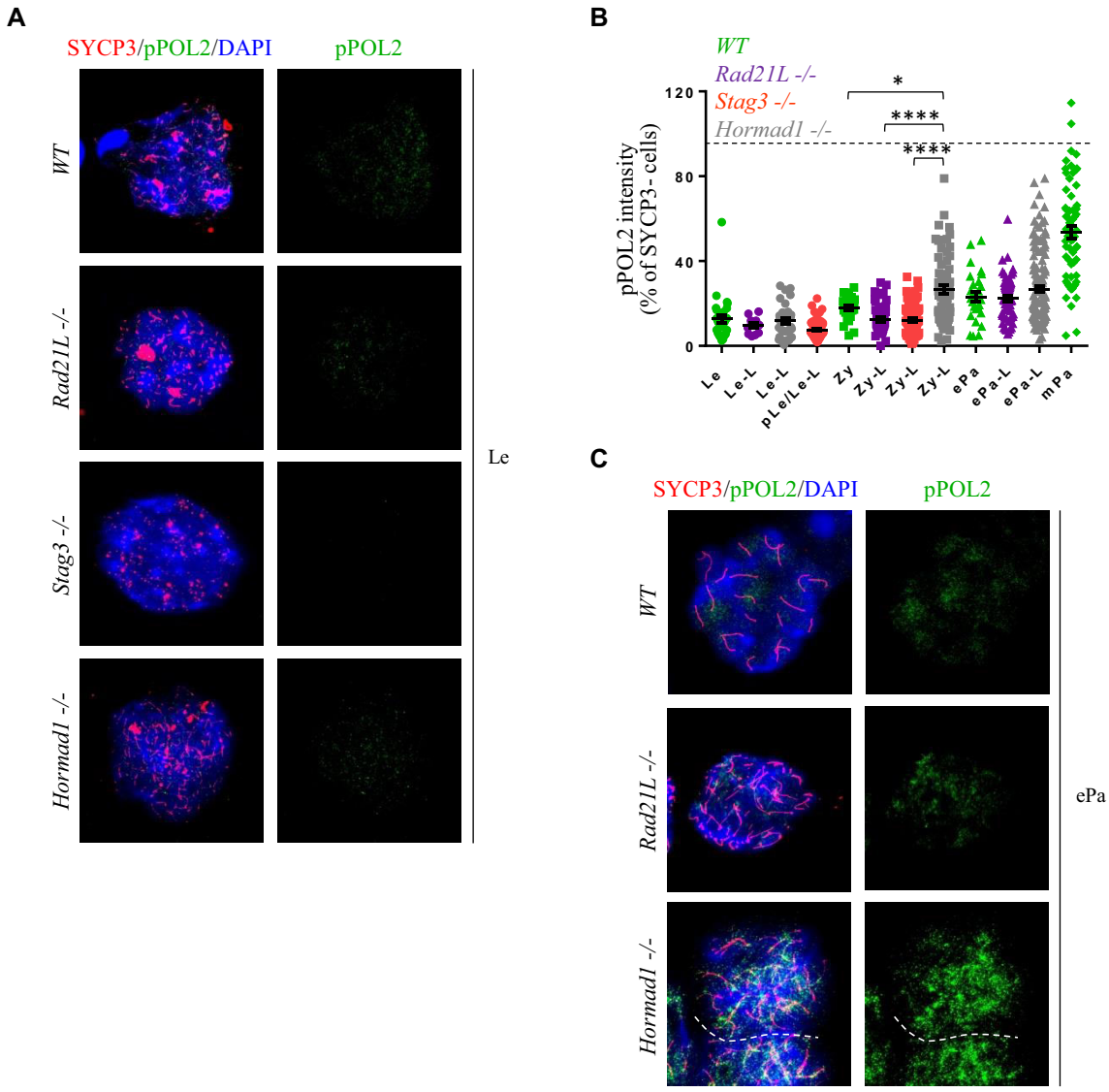

Figure 3. Co-labelling with SYCP3 and pPOL2 on spermatocyte chromosome spreads of WT and KO mice *Rad21L -/-*, *Stag3 -/-*, and *Hormad1 -/-* (**A**). Quantification of pPOL2 intensity evidenced a weak signal at leptotene (Le) or leptotene-like (Le-L) stage (**B**). pPOL2 intensity is normalized to mitotic cells (100%, dashed line). Black bars represent mean ± sem. WT: $n = 5$; *Hormad1 -/-*: $n = 3$; *Stag3 -/-*: $n = 3$; and *Rad21L -/-*: $n = 3$. $^{*}P < .05$, $^{****}P < .0001$ (unpaired *t*-test). *In Hormad1 -/-*, some early pachytene (ePa) spermatocytes are strongly stained for pPOL2 in comparison to WT and *Rad21L -/-* (**C**).

Stra8 regulates EMLT induction

Given that EMLT occurs around meiotic entry, we analysed pPOL2 in germ cells mutant for the main regulators of meiotic initiation. *Stra8* is a key gene involved in mitotic to meiotic transition [50,51]. It is initially expressed in A spermatogonia following their differentiation and it is strongly expressed during pre-leptotene stage. STRA8 regulates the transcription of large sets of genes. Analysis of *Stra8* null mutant mice revealed the absence of the primary induction of EMLT. In fact, quantification of pPOL2 in testis sections of *Stra8*$^{-/-}$ mice showed a high level of pPOL2 in intermediate and B spermatogonia and in pre-leptotene spermatocytes when compared to corresponding stages in WT (Fig. 5 and Supplementary Fig. S16 and S17A). Interestingly, measure of pPOL2 intensity in *Stra8-/-* ovaries also showed a higher level of pPOL2 in leptotene-like oocytes (Supplementary Fig. S17B). MEIOC is another key factor that regulates meiosis initiation through modulation of post-transcriptional events. Contrarily to *Stra8*, genetic depletion of *Meioc* did not modify EMLT (Fig. 5 and Supplementary Fig. S17A), indicating that simply impairing meiotic entry was insufficient to delay the transcriptional arrest. Thus, establishment of meiotic program through STRA8 is important for the correct temporal regulation of EMLT.

RNAs are massively stabilized during EMLT

The combined duration of leptotene and zygotene stages is expected to be ~3 days. How do cells survive and progress through these stages with hardly any transcription is intriguing. Comparing the 'spliced' and 'unspliced' expression profiles, which reflect the presence of transcripts and nascent transcription, respectively, we observed that both decreased notably at meiotic entry (Fig. 6A). However, the decrease of 'spliced' RNAs was less pronounced indicating that some transcripts persisted. As an example, the *Rplp0* housekeeping gene displayed a 20-fold decrease in transcription while

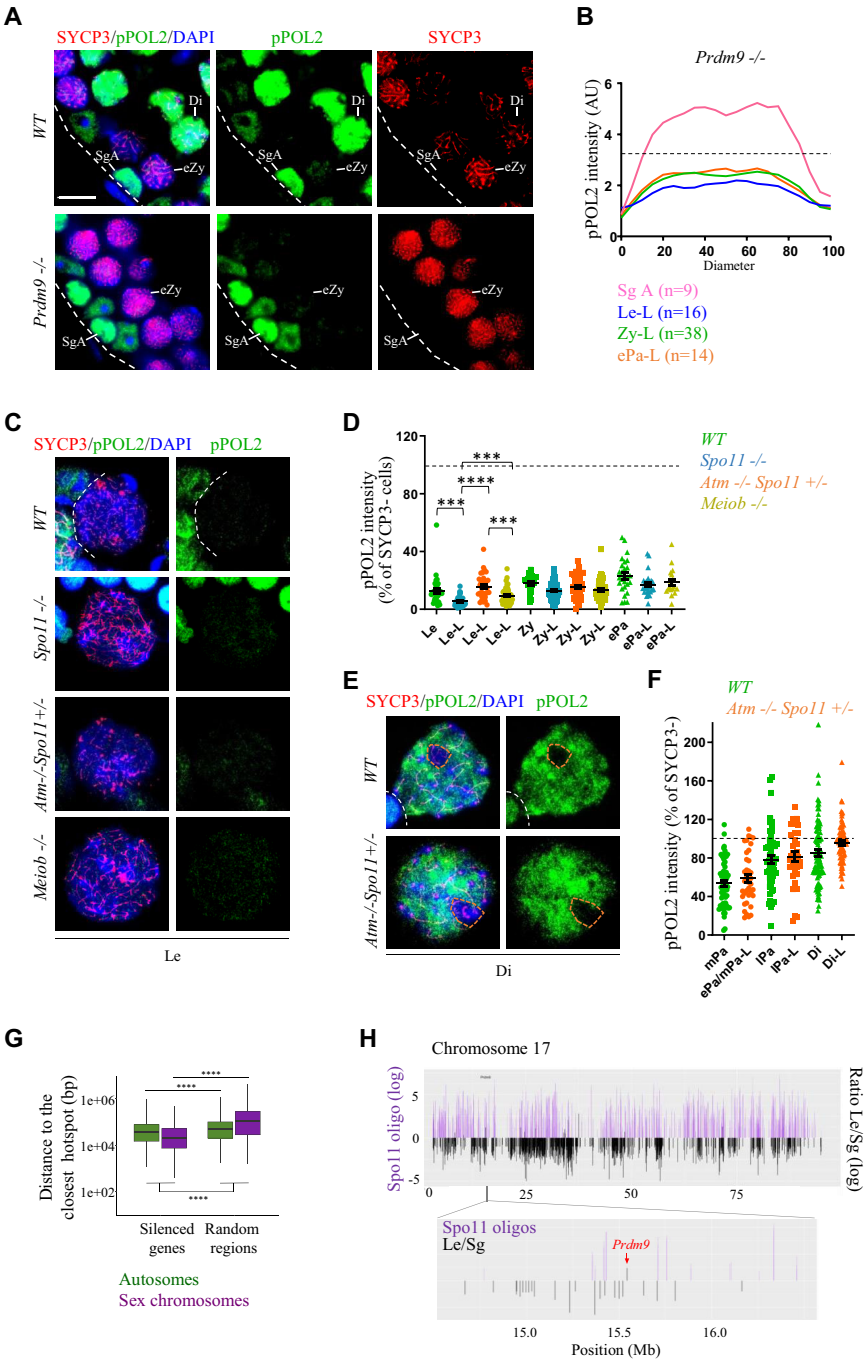

Figure 4. WT and Prdm9 -/- testis sections stained for SYCP3 (red) and pPOL2 (green) (**A**). Prophase I cells are identified thanks to SYCP3 and DNA is stained with DAPI. SgA = spermatogonia A; eZy = early zygotene; and Di = diplotene. Dotted white curbs delimit seminiferous tubules. Scale bar = 10 μm. Line plot quantification of pPOL2 intensity in Prdm9 null mutants (Prdm9 -/-, $n = 2$ mice) (**B**). For quantification, a line was traced randomly through nucleus and for each point along the line, intensity was quantified using ImageJ software (plot profile). The horizontal axis represents the diameter of the cells. Each line represents the average of pPOL2 intensity of several cells. Leptotene-like (Le-L, $n = 16$), zygotene-like (Zy-L, $n = 38$), and early-pachytene like (ePa-L, $n = 14$) cells are less stained for pPOL2 than A spermatogonia (Sg A, $n = 9$). AU = arbitrary units. Immunofluorescence staining for SYCP3 and pPOL2 of spermatocyte chromosome spreads of WT and KO mice *Meiob*-/-, *Spo11*-/-, and double transgenic KO mice *Atm*-/- *Spo11*+/- (**C**). Quantification of pPOL2 intensity indicates that all mice show weak pPOL2 signal at leptotene (Le) stage (**D**). pPOL2 intensity is normalized to mitotic cells (100%, black dashed line). Black bars represent mean ± sem. WT: $n = 5$; *Meiob* -/-: $n = 3$; *Spo11* -/-: $n = 3$; and *Atm*-/-*Spo11*+/-: $n = 3$. $^{***}P < .001$, $^{****}P < .0001$ (unpaired *t*-test). Both WT and *Atm* -/- *Spo11* +/- mice show high pPOL2 staining at diplotene stage (Di), except for sex body (orange dotted line) (**E**). Quantification of pPOL2 intensity on spermatocyte chromosome spreads (**F**). Boxplot of the distance (log10) to the closest hotspot (in bp) for the 11 660 'silenced' genes and 1000 random intergenic regions according to their chromosomal location (autosomes in green and sex chromosomes in purple) (**G**). DSBs hotspot data as defined by anti-DMC1 ssDNA sequencing data in C57BL/6J mice was downloaded from GEO (GSE75419). Two-tailed Wilcoxon tests were used to compare the distance to the nearest hotspot in the different sets of genes. $^{****}P < 0.0001$. Illustration of the distribution of DNA DSBs defined by mapping SPO11 oligonucleotides (Spo11 oligo, purple) and transcriptional changes between leptotene stage and spermatogonia (Ratio Le/Sg, black) along mouse chromosome 17 (**H**). Bottom image is a two Mb zoom centered on the 'escaping' gene *Prdm9*. Coordinate of SPO11-oligo were obtained from Lange *et al.* Transcriptional changes were calculated from scRNA-seq data (ratio Le/Diff Sg1).

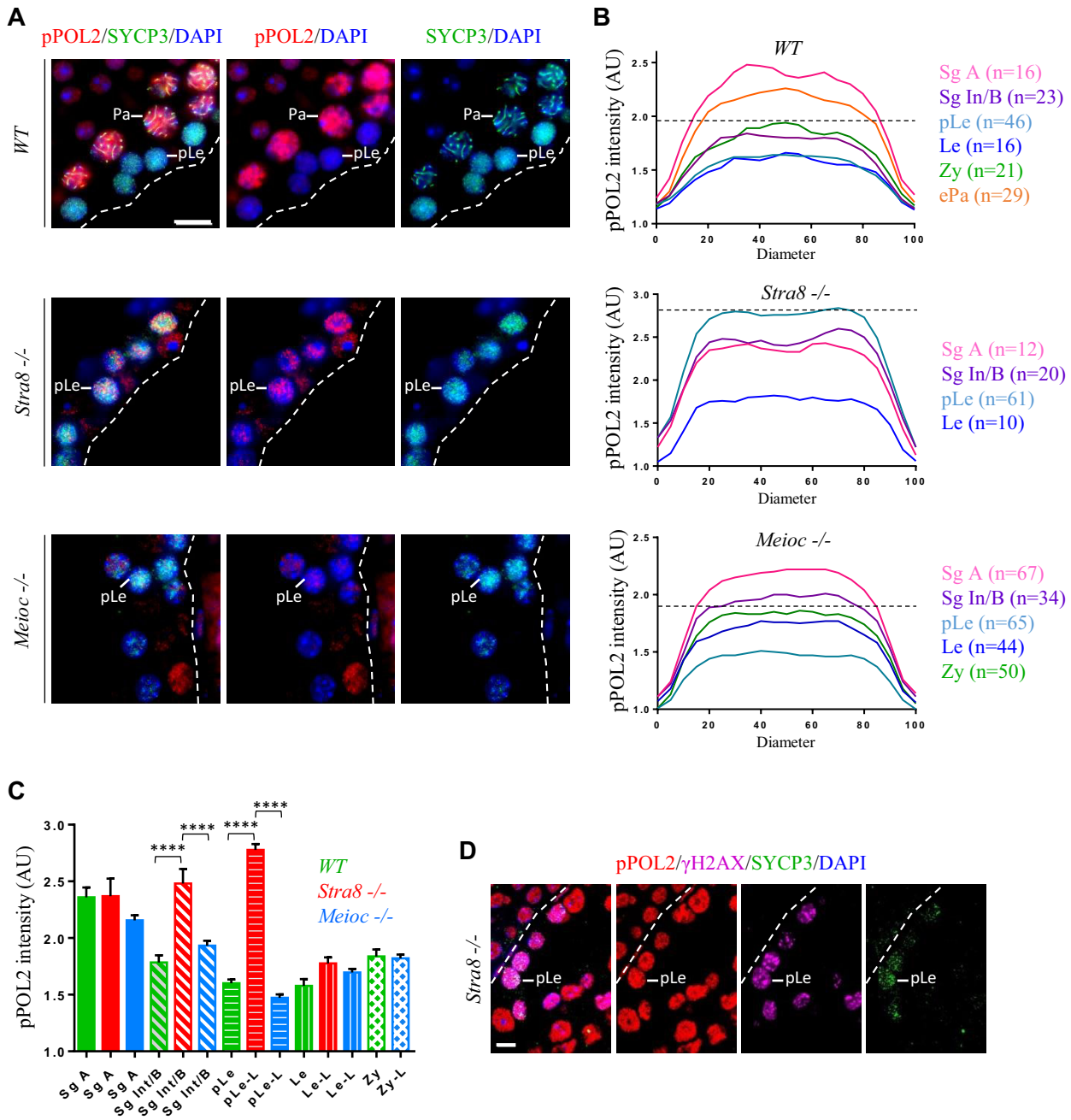

Figure 5. Co-immunofluorescence staining of pPOL2 with SYCP3 on testis sections from WT and *Stra8* -/- and *Meioc* -/- mice (**A**). Preleptotene (pLe) cells are indicated and DNA is stained with DAPI [panels (A) and (D)]. Scale bar = 10 μm. Line plot quantification of pPOL2 intensity in WT (upper), *Stra8* -/- (middle), and *Meioc* -/- (lower) (**B**). The horizontal axis represents the diameter of the cells. (AU = arbitrary units, normalization was based on background level). Legend is as in Fig. 1B. The number of analysed cells is indicated in brackets for each cell type. Mean pPOL2 intensity within nuclei (**C**). Columns represent mean ± sem. In *Stra8* -/-, Sg Int/B, and pLe cells are more stained for pPOL2 than in WT and *Meioc* -/-. AU = arbitrary units. ****$P < 0.0001$ (ordinary one-way ANOVA, multiple comparisons). Co-labelling of pPOL2, γH2AX, and SYCP3 in *Stra8* -/- testes sections (**D**). pLe cells in *Stra8* -/- testes, stained for γH2AX and SYCP3, are not subjected to EMLT and show pPOL2 staining. Scale bar = 5 μm.

its mRNA merely decreased two-fold during EMLT (i.e. in leptotene, unspliced mRNA equal to 4.3% versus spliced mRNA equal to 39% of the value in undifferentiated spermatogonia). We thus considered the ratio of 'spliced' to 'unspliced' expression levels to obtain a proxy of RNA stability. An increase of RNA stability was observed during EMLT for both 'silenced' and 'escaping' genes in scRNA-seq data (Fig. 6A). Similar results were observed using the EU-RNA-seq dataset (Supplementary Fig. S18). We hypothesized that this stabilization may be involved in launching the meiotic program and thus focused on a list of genes highly expressed during meiotic entry (Fig. 6B and Supplementary Table S3); these were previously published genes expressed specifically from pre-meiotic cells and onwards [52] completed by five additional genes we systematically observed at meiotic entry in our transcriptomic analyses (*Fmr1*, *Ly6k*, *Sirt7*, *Taf4b*, and *Terb2*). These 91 genes were grouped based on their nascent transcription profile (set 1 = early transcribed genes;

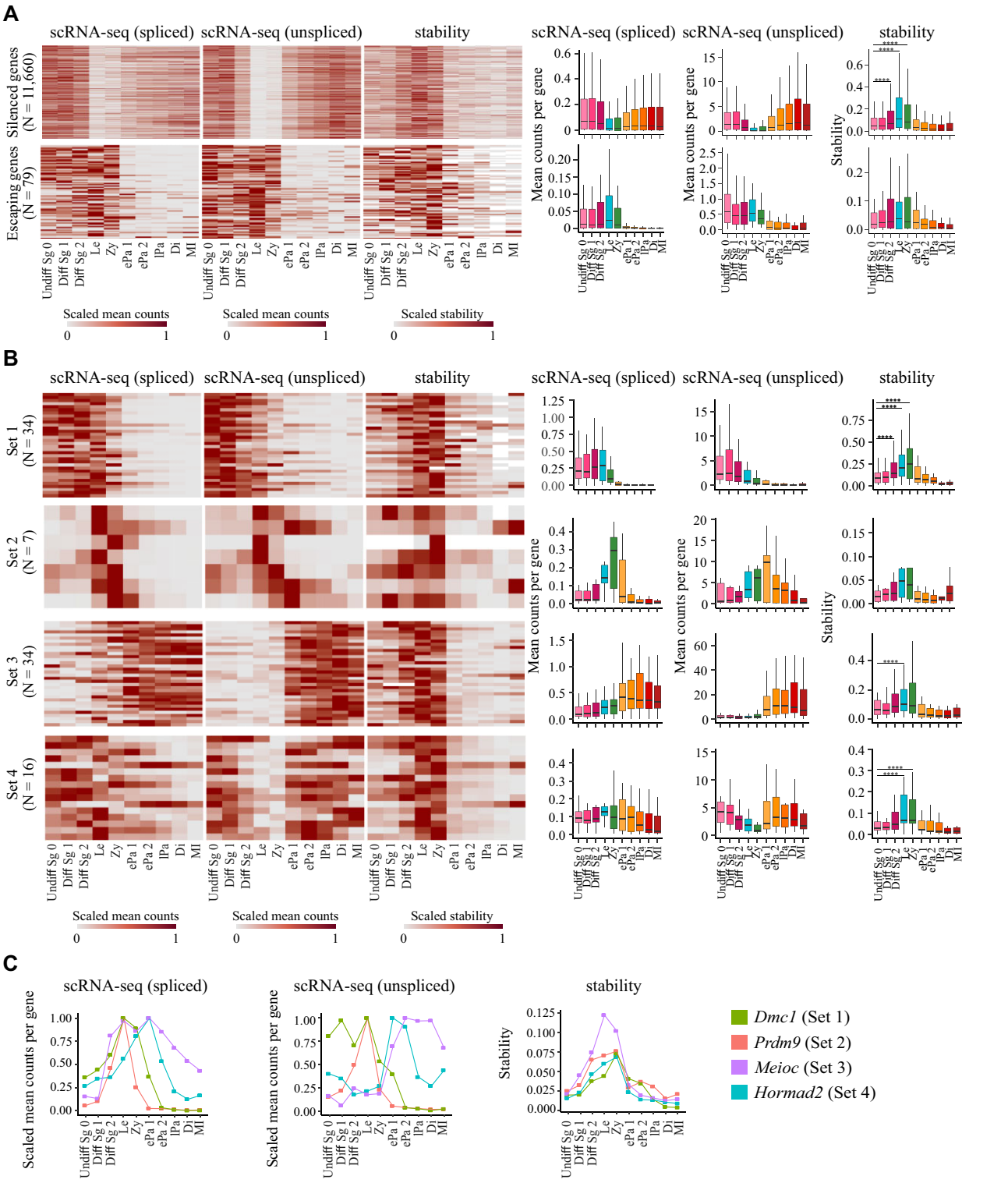

Figure 6. Heatmaps and boxplots of the spliced (left) and unspliced (middle) expression profiles and the stability (right) of 'Silenced' (top) and 'Escaping' (bottom) genes (**A**), and of four sets of early meiotic genes (**B**). Set 1 = early transcribed genes; set 2 = genes transcribed during Le/Zy; set 3 = late transcribed genes; and set 4 = genes silenced during Le/Zy. The 'spliced' and 'unspliced' expression profiles reflect transcription and nascent transcription, respectively, while the 'stability' is the ratio of 'spliced' to 'unspliced' expression levels. In the heatmaps, each row represents a gene, and each column represents a specific spermatogenic cell population. For heatmaps, 'spliced' and 'unspliced' expression values of each gene were scaled between [0;1] using a zero-max scale (0 = 0; maximum value = 1), stability of each gene was scaled between [0;1] using a conventional scaling (minimum value = 0; maximum value = 1). Boxplots display the average counts per gene for the 'spliced' and 'unspliced' dataset, and stability per gene. Undiff Sg 0 = undifferentiated spermatogonia; Diff Sg = differentiated spermatogonia; Le = leptotene; Zy = zygotene; ePa = early pachytene spermatocytes; lPa = late pachytene; Di = diplotene spermatocytes; and MI = metaphase I spermatids. Gene expression and stability profiles of four representative genes from undifferentiated spermatogonia to metaphase I spermatocytes (**C**). Plots represent the scaled average counts per gene from spliced (left) and unspliced (middle) data, and the resulting stability (right). Each of the selected genes (*Dmc1*, *Prdm9*, *Meioc*, and *Hormad2*) belong to one of the four sets of meiotic genes presented in panel (B).

set 2 = genes transcribed during Le/Zy; set 3 = late transcribed genes; and set 4 = genes silenced during Le/Zy). RNA stability during EMLT was also observed for the four sets of genes. These observations were also confirmed in the bulk approach with sorted cells (Supplementary Fig. S19). Four well-known meiotic genes (*Dmc1 Prdm9, Meioc*, and *Hormad2*), representing each set, were used to exemplify this (Fig. 6C). Although these displayed distinct nascent transcription profiles (unspliced RNA), they were robustly and simultaneously expressed in early meiosis (spliced RNA), with their stability sharply increasing in leptotene and zygotene cells. These results suggest that the global stabilization of mRNA during EMLT and meiotic entry may facilitate the synchronized rise of meiotic gene expression.

Discussion

During the reproductive cycle, several transcriptional silencing events occur in germ cells and in the zygote [53–55]. In this study, we characterized EMLT, a genome-wide silencing phenomenon during early meiotic prophase I. EMLT was dependent of the meiotic gatekeeper STRA8 but did not rely on other key events of meiotic prophase I for its establishment.

Examples of genome-wide transcriptional arrest are uncommon and notably associated with gametogenesis. Such occurrences have been well-documented post-fertilization during the early embryonic development and in primordial germ cells. The tight packaging of chromatin in the spermatozoa also induces a transcriptional silencing, though the cause is evident in this context [56]. Here, we provide a detailed characterization of the silencing event occurring at the time of meiotic entry, adding new insights to its understanding. The reason why germ cells are that frequently subjected to transcriptional arrests remains unclear. One may consider that among all cells, germ cells must transition between highly different states, justifying an extreme transcriptional dynamic. Indeed, germ cells need to undergo various specifications: first PGCs are committed to the germ lineage; then they shift from a mitotic to a meiotic program; and later, post-meiotic male germ cells undergo a massive cellular reorganization. Finally, after the fusion of gamete genomes, the zygote must regain totipotency. Interestingly, all these changes are accompanied by major chromatin remodelling events, such as DNA methylation erasure [57], meiotic recombination [58], histone to protamine transition [59], or diploidization. Of note, methylation erasure occurs in PGCs, during the first embryonic cleavages and at the time of meiotic entry [60]. A simple view may accept that a quiet chromatin is a conductive environment for such events, and that an active transcriptional machinery could potentially interfere with these processes.

Recently, low transcription during leptonema and zygonema has also been reported in a study proposing it may reflect a promoter proximal paused state of POL2 [61]. Another recent study described a POL2 pausing in spermatogonia [62]. It is therefore conceivable that the absence of POL2 detection on chromatin in our work merely reflects a paused state.

EMLT occurring around the mitotic–meiotic switch is intriguing. Here we reported, through the analysis of several meiotic mutants, that this transcriptional arrest occurred similarly when the specific meiotic chromosomal architecture or DSB program was impaired. Similarly, it has previously been reported that unresolved DSBs or severe synaptic defects do not alter the pattern of pPOL2 in leptotene- and zygotene-like spermatocytes in various mutant mice [48]. Cohesins shape the chromosomal architecture and have been proposed as key regulators of transcription [63–65]. The involvement of specific cohesins during meiosis would be a tentative hypothesis to explain a change in transcriptional activity. However, neither *Stag3* nor *Rad21L* depletion impacted EMLT, despite the structure of meiotic chromosomes being deeply altered in such mutants. On the other hand, transcription has been proven to move cohesins [66, 67]. One may thus speculate that a reverse relationship exists between EMLT and cohesins. During early meiosis, the lack of transcription may provide some stability to cohesins to initiate the axial-loop structure and the formation of the axial element formation. Another significant event occurring during early meiosis is the formation and repair of hundreds of programmed DSBs. In somatic cells, DNA damage repair has been reported to interfere with transcription in many ways, likely because both phenomena require an accessible chromatin [68]. Initially, a rather straight hypothesis would have been that DSB patterning, formation, signaling or repair might trigger a transcriptional arrest. The analysis *of Prdm9*, *Spo11*, *Atm/Atr*, and *Meiob* mutants contradicts such hypothesis. A reverse relationship, i.e. that active transcription might interfere with the proper generation or repair of programmed DSBs, may then be considered. In this line, it is worth quoting that DSB sites are marked by H3K4me3, this histone modification is also the one retrieved in the promoters of transcriptionally active genes. A speculative assumption could be that sharing such a mark is risky and may confuse the recruitment of the DSB forming machinery. Therefore, a state of near-extinct transcription might favour the proper localization of DSB in hotspots outside gene promoters. This hypothesis gains support from our observation that recombination occurred preferentially in transcriptionally silent regions and is in agreements with a publication indicating that DSBs occur in untranscribed genomic regions [61]. In the same line, it was also recently proposed that paused POL2 sites in spermatogonia correlate with those of DSBs induced by SPO11 in spermatocytes [62].

To test such hypotheses, it would be necessary to manipulate EMLT and this implies understanding its mechanisms or trigger. Here we report that EMLT is significantly delayed in absence of *Stra8*. STRA8 controls the expression of the near complete meiotic gene network. Specifically, it has recently been shown to amplify a pre-existing meiotic program [10]. This aligns with the concept that STRA8 might regulate a meiotic factor that causes EMLT. In the absence of *Stra8*, such a factor would be expressed at low levels, thus delaying EMLT. Unfortunately, identifying this factor within the thousands of genes that compose the STRA8-dependent meiotic program remains a challenge. The mechanism causing EMLT also remains evasive. We report here that this mechanism differs from MSCI that is regulated by DSB signaling, asynapsis and the SETDB1 histone methylase. However, the absence of recruitment of POL2 and pPOL2 is a common feature shared by MSCI and EMLT. This reinforces the view that MSCI might be a gonosome-specific prolongation of a wider phenomenon, EMLT [19]. In this line, it could be conceived that the histone mark repressing transcription during MSCI would also be shared with EMLT. H3K9me3 is the mark deposited by SETDB1 involved in instructing MSCI [13], though its exact role has recently been debated [16]. Interestingly, H3K9me3 is also present on silent chromosomes

during early prophase I, making it a likely candidate to induce EMLT. In this scenario, EMLT would rely on a different methylase which may explain that few genes on sex chromosomes are differentially regulated during EMLT and MSCI. Of note, H3K9me3 may not be the sole signal involved and additional chromatin modifications may be involved. Notably, mono-methylation of H3K4 may also be correlated to EMLT [19, 48]. Furthermore, other differences, especially regarding POL2 dynamics, exist between EMLT and MSCI.

Gene expression can be considered as the outcome of transcription and mRNA decay rates. Our work also revealed that EMLT is accompanied by a wide event of RNA stabilization. This stabilization event likely buffered the decrease in transcription at meiotic onset. This aligns with a report indicating that in human cell lines, global transcriptional shutdown leads to stabilization of nearly all of transcripts through inhibition of the mRNA degradation machinery [69]. Whether a similar relationship between low transcription and RNA stability exist in germ cells is a point that warrants future studies. Strikingly, when assessing the transcription of genes specifically expressed at the onset of meiosis, we observed that many (84/91) were predominantly transcribed at other stages. For most of them (sets 1, 3, and 4), their transcription decreased at the time of meiotic entry. Thus, the increased expression of these meiotic genes is mainly due to changes in RNA stability. Meiotic licensing depends upon *Dazl* that is expressed early during fetal life, yet male germ cells do not initiate meiosis before post-natal life [70]. This allows speculation that part of the meiotic program might be set up early, and that the decision to actually initiate meiosis requires the stabilization of RNA to allow meiotic genes transcribed at low levels to reach a sufficient level. The second effect of this massive RNA stabilization we observed is likely to synchronize various 'meiotic subprograms' to provide a timely expression of all genes needed in early meiotic prophase I. Such a hypothesis positions mRNA stabilization as a key player orchestrating meiotic entry. In *Schizosaccharomyces pombe*, the proper timing of meiosis is controlled by the sequestration of the RNA-binding protein Mmi1, that triggers the degradation of some meiotic RNA during mitotic growth [71]. In *Caenorhabditis elegans*, meiotic entry is partly controlled by a poly (A)-polymerase, GLD-2, that increases mRNA stability [72, 73]. Thus, a change of RNA stability might be an ancestral mechanism controlling the mitotic–meiotic switch that has yet poorly been investigated in mammals.

In conclusion, our study provides an in-depth description of the genome-wide silencing event reported to occur during leptotene and zygotene stages. We quantified this event and proved it initiates prior to meiotic entry and is regulated by the meiotic gatekeeper, STRA8. This silencing and the accompanying RNA stabilization are key to ensure a robust switch from the mitotic to the meiotic program. Future research will have to identify the specific mechanisms responsible for EMLT and through their manipulation it is expected that the reasons for such a major genome silencing will be unveiled.

Acknowledgements

The authors sincerely thank Dr J.M. Turner for helpful discussion, advices, and providing the samples from *Setb1* and *Atr/Atm* mutant mice. We are indebted to Dr F. Baudat and Dr B. de Massy and Dr C. Grey for the generous provision of testicular samples from *Spo11*, *Prdm9*, and mice. Flow cytometry and cell sorting were carried out at the iRCM Flow Cytometry Shared Resource. We also thank the team within the animal housing facility at the iRCM, particularly V. Neuville and the Centre National de Recherche en Génomique Humaine for sequencing, D. Moison and S. Tourpin for her technical assistance and A. Gouret for her secretarial assistance.

Author contributions: L.B. designed and performed most of the molecular, cell, and animal experiments with V.C., M-J.G., S.M., E.L., and I.D. E.C.S.P. and A.R. performed the single-cell transcriptome analysis and nascent RNA analysis. L.B., A.T., and A.M.P. helped design the animal study. A.R., E.M., A.T., and A.M.P. monitored the study. F.C. and G.L. conceived the study, interpreted the experiments, and wrote the manuscript with inputs from the other authors.

Supplementary data

Supplementary data is available at NAR online.

Conflict of interest

All authors declare that they have no conflicts of interest.

Funding

This research was supported by the Agence Nationale de la Recherche (ANR-18-CE14-0038 and ANR-20-CE14-0022) and by the Ministerio de Ciencia e Innovación (PID2020-120326RB-I00) and Junta de Castilla y León (Unidad de Investigación Consolidada 066, CSI148P20 and CSI017P23). Funding to pay the Open Access publication charges for this article was provided by University dotation or research contract.

Data availability

The data underlying this article will be shared upon request to the corresponding authors. The sequencing datasets have been deposited in the GEO with accession number GSE261062.

References

1. Griswold MD. Spermatogenesis: the commitment to meiosis. *Physiol Rev* 2016;**96**:1–17. https://doi.org/10.1152/physrev.00013.2015
2. de Rooij DG. Proliferation and differentiation of spermatogonial stem cells. *Reproduction* 2001;**121**:347–54. https://doi.org/10.1530/rep.0.1210347
3. Feng C-W, Bowles J, Koopman P. Control of mammalian germ cell entry into meiosis. *Mol Cell Endocrinol* 2014;**382**:488–97. https://doi.org/10.1016/j.mce.2013.09.026
4. Hermo L, Pelletier R-M, Cyr DG *et al.* Surfing the wave, cycle, life history, and genes/proteins expressed by testicular germ cells. Part 2: changes in spermatid organelles associated with development of spermatozoa. *Microsc Res Tech* 2010;**73**:279–319. https://doi.org/10.1002/jemt.20787
5. Chalmel F, Rolland AD. Linking transcriptomics and proteomics in spermatogenesis. *Reproduction* 2015;**150**:R149–57. https://doi.org/10.1530/REP-15-0073
6. Margolin G, Khil PP, Kim J *et al.* Integrated transcriptome analysis of mouse spermatogenesis. *BMC Genomics* 2014;**15**:39. https://doi.org/10.1186/1471-2164-15-39
7. Murat F, Mbengue N, Winge SB *et al.* The molecular evolution of spermatogenesis across mammals. *Nature* 2023;**613**:308–16. https://doi.org/10.1038/s41586-022-05547-7

8. Naro C, Jolly A, Di Persio S *et al.* An orchestrated intron retention program in meiosis controls timely usage of transcripts during germ cell differentiation. *Dev Cell* 2017;**41**:82–93. https://doi.org/10.1016/j.devcel.2017.03.003
9. Turner JMA. Meiotic silencing in mammals. *Annu Rev Genet* 2015;**49**:395–412. https://doi.org/10.1146/annurev-genet-112414-055145
10. Kojima ML, de Rooij DG, Page DC. Amplification of a broad transcriptional program by a common factor triggers the meiotic cell cycle in mice. *eLife* 2019;**8**:e43738. https://doi.org/10.7554/eLife.43738
11. Cooper TJ, Garcia V, Neale MJ. Meiotic DSB patterning: a multifaceted process. *Cell Cycle* 2016;**15**:13–21. https://doi.org/10.1080/15384101.2015.1093709
12. Lange J, Yamada S, Tischfield SE *et al.* The landscape of mouse meiotic double-strand break formation, processing, and repair. *Cell* 2016;**167**:695–708. https://doi.org/10.1016/j.cell.2016.09.035
13. Hirota T, Blakeley P, Sangrithi MN *et al.* SETDB1 links the meiotic dna damage response to sex chromosome silencing in mice. *Dev Cell* 2018;**47**:645–59. https://doi.org/10.1016/j.devcel.2018.10.004
14. ElInati E, Russell HR, Ojarikre OA *et al.* DNA damage response protein TOPBP1 regulates X chromosome silencing in the mammalian germ line. *Proc Natl Acad Sci USA* 2017;**114**:12536–41. https://doi.org/10.1073/pnas.1712530114
15. Royo H, Prosser H, Ruzankina Y *et al.* ATR acts stage specifically to regulate multiple aspects of mammalian meiotic silencing. *Genes Dev* 2013;**27**:1484–94. https://doi.org/10.1101/gad.219477.113
16. Abe H, Yeh Y-H, Munakata Y *et al.* Active DNA damage response signaling initiates and maintains meiotic sex chromosome inactivation. *Nat Commun* 2022;**13**:7212. https://doi.org/10.1038/s41467-022-34295-5
17. Abby E, Tourpin S, Ribeiro J *et al.* Implementation of meiosis prophase I programme requires a conserved retinoid-independent stabilizer of meiotic transcripts. *Nat Commun* 2016;**7**:10324. https://doi.org/10.1038/ncomms10324
18. Monesi V. Ribonucleic acid synthesis during mitosis and meiosis in the mouse testis. *J Cell Biol* 1964;**22**:521–32. https://doi.org/10.1083/jcb.22.3.521
19. Page J, de la Fuente R, Manterola M *et al.* Inactivation or non-reactivation: what accounts better for the silence of sex chromosomes during mammalian male meiosis? *Chromosoma* 2012;**121**:307–26. https://doi.org/10.1007/s00412-012-0364-y
20. Ernst C, Eling N, Martinez-Jimenez CP *et al.* Staged developmental mapping and X chromosome transcriptional dynamics during mouse spermatogenesis. *Nat Commun* 2019;**10**:1251. https://doi.org/10.1038/s41467-019-09182-1
21. Hogarth CA, Evanoff R, Mitchell D *et al.* Turning a spermatogenic wave into a tsunami: synchronizing murine spermatogenesis using WIN 18,446. *Biol Reprod* 2013;**88**:40. https://doi.org/10.1095/biolreprod.112.105346
22. Bastos H, Lassalle B, Chicheportiche A *et al.* Flow cytometric characterization of viable meiotic and postmeiotic cells by Hoechst 33342 in mouse spermatogenesis. *Cytometry A* 2005;**65A**:40–9. https://doi.org/10.1002/cyto.a.20129
23. Souquet B, Abby E, Hervé R *et al.* MEIOB targets single-strand DNA and is necessary for meiotic recombination. *PLoS Genet* 2013;**9**:e1003784. https://doi.org/10.1371/journal.pgen.1003784
24. Widger A, Mahadevaiah SK, Lange J *et al.* ATR is a multifunctional regulator of male mouse meiosis. *Nat Commun* 2018;**9**:2621. https://doi.org/10.1038/s41467-018-04850-0
25. Diagouraga B, Clément JAJ, Duret L *et al.* PRDM9 methyltransferase activity is essential for meiotic DNA double-strand break formation at its binding sites. *Mol Cell* 2018;**69**:853–65. https://doi.org/10.1016/j.molcel.2018.01.033
26. Daniel K, Lange J, Hached K *et al.* Meiotic homologue alignment and its quality surveillance are controlled by mouse HORMAD1. *Nat Cell Biol* 2011;**13**:599–610. https://doi.org/10.1038/ncb2213
27. Herrán Y, Gutiérrez-Caballero C, Sánchez-Martín M *et al.* The cohesin subunit RAD21L functions in meiotic synapsis and exhibits sexual dimorphism in fertility. *EMBO J* 2011;**30**:3091–105. https://doi.org/10.1038/emboj.2011.222
28. Llano E, Gomez-H L, García-Tuñón I *et al.* STAG3 is a strong candidate gene for male infertility. *Hum Mol Genet* 2014;**23**:3421–31. https://doi.org/10.1093/hmg/ddu051
29. Dereli I, Stanzione M, Olmeda F *et al.* Four-pronged negative feedback of DSB machinery in meiotic DNA-break control in mice. *Nucleic Acids Res* 2021;**49**:2609–28. https://doi.org/10.1093/nar/gkab082
30. McCarthy DJ, Campbell KR, Lun ATL *et al.* Scater: pre-processing, quality control, normalization and visualization of single-cell RNA-seq data in R. *Bioinformatics* 2017;**33**:1179–86. https://doi.org/10.1093/bioinformatics/btw777
31. McGinnis CS, Murrow LM, Gartner ZJ. DoubletFinder: doublet detection in single-cell RNA sequencing data using artificial nearest neighbors. *Cell Syst* 2019;**8**:329–37. https://doi.org/10.1016/j.cels.2019.03.003
32. Lun ATL, Bach K, Marioni JC. Pooling across cells to normalize single-cell RNA sequencing data with many zero counts. In: Azevedo VADC, Barh D (eds.), *Single-cell Omics: Technological Advances and Applications*. San Diego, CA: Academic Press Inc, London, 2019, 75–89. https://doi.org/10.1186/s13059-016-0947-7
33. Stuart T, Butler A, Hoffman P *et al.* Comprehensive integration of single-cell data. *Cell* 2019;**177**:1888–1902. https://doi.org/10.1016/j.cell.2019.05.031
34. La Manno G, Soldatov R, Zeisel A *et al.* RNA velocity of single cells. *Nature* 2018;**560**:494–8. https://doi.org/10.1038/s41586-018-0414-6
35. Smagulova F, Brick K, Pu Y *et al.* The evolutionary turnover of recombination hot spots contributes to speciation in mice. *Genes Dev* 2016;**30**:266–80. https://doi.org/10.1101/gad.270009.115
36. Quinlan AR, Hall IM. BEDTools: a flexible suite of utilities for comparing genomic features. *Bioinformatics* 2010;**26**:841–2. https://doi.org/10.1093/bioinformatics/btq033
37. Chen Y, Lyu R, Rong B *et al.* Refined spatial temporal epigenomic profiling reveals intrinsic connection between PRDM9-mediated H3K4me3 and the fate of double-stranded breaks. *Cell Res* 2020;**30**:256–68. https://doi.org/10.1038/s41422-020-0281-1
38. Teletin M, Vernet N, Ghyselinck NB *et al.* Roles of retinoic acid in germ cell differentiation. *Curr Top Dev Biol* 2017;**125**:191–225. https://doi.org/10.1016/bs.ctdb.2016.11.013
39. Gil-Fernández A, Saunders PA, Martín-Ruiz M *et al.* Meiosis reveals the early steps in the evolution of a neo-XY sex chromosome pair in the African pygmy mouse Mus minutoides. *PLoS Genet* 2020;**16**:e1008959. https://doi.org/10.1371/journal.pgen.1008959
40. Marín-Gual L, González-Rodelas L, Pujol G *et al.* Strategies for meiotic sex chromosome dynamics and telomeric elongation in Marsupials. *PLoS Genet* 2022;**18**:e1010040. https://doi.org/10.1371/journal.pgen.1010040
41. van der Heijden GW, Derijck AAHA, Pósfai E *et al.* Chromosome-wide nucleosome replacement and H3.3 incorporation during mammalian meiotic sex chromosome inactivation. *Nat Genet* 2007;**39**:251–8. https://doi.org/10.1038/ng1949
42. Llano E, Herrán Y, García-Tuñón I *et al.* Meiotic cohesin complexes are essential for the formation of the axial element in mice. *J Cell Biol* 2012;**197**:877–85. https://doi.org/10.1083/jcb.201201100
43. Hamer G, Roepers-Gajadien HL, van Duyn-Goedhart A *et al.* DNA double-strand breaks and gamma-H2AX signaling in the testis. *Biol Reprod* 2003;**68**:628–34. https://doi.org/10.1095/biolreprod.102.008672
44. Baudat F, Buard J, Grey C *et al.* PRDM9 is a major determinant of meiotic recombination hotspots in humans and mice. *Science* 2010;**327**:836–40. https://doi.org/10.1126/science.1183439

45. Parvanov ED, Petkov PM, Paigen K. Prdm9 controls activation of mammalian recombination hotspots. *Science* 2010;**327**:835. https://doi.org/10.1126/science.1181495
46. Baudat F, Manova K, Yuen JP *et al.* Chromosome synapsis defects and sexually dimorphic meiotic progression in mice lacking Spo11. *Mol Cell* 2000;**6**:989–98. https://doi.org/10.1016/S1097-2765(00)00098-8
47. Romanienko PJ, Camerini-Otero RD. The mouse Spo11 gene is required for meiotic chromosome synapsis. *Mol Cell* 2000;**6**:975–87. https://doi.org/10.1016/S1097-2765(00)00097-6
48. de la Fuente R, Pratto F, Hernández-Hernández A *et al.* Epigenetic dysregulation of mammalian male meiosis caused by interference of recombination and synapsis. *Cells* 2021;**10**:2311. https://doi.org/10.3390/cells10092311
49. Barchi M, Mahadevaiah S, Di Giacomo M *et al.* Surveillance of different recombination defects in mouse spermatocytes yields distinct responses despite elimination at an identical developmental stage. *Mol Cell Biol* 2005;**25**:7203–15. https://doi.org/10.1128/MCB.25.16.7203-7215.2005
50. Anderson EL, Baltus AE, Roepers-Gajadien HL *et al.* Stra8 and its inducer, retinoic acid, regulate meiotic initiation in both spermatogenesis and oogenesis in mice. *Proc Natl Acad Sci USA* 2008;**105**:14976–80. https://doi.org/10.1073/pnas.0807297105
51. Koubova J, Menke DB, Zhou Q *et al.* Retinoic acid regulates sex-specific timing of meiotic initiation in mice. *Proc Natl Acad Sci USA* 2006;**103**:2474–9. https://doi.org/10.1073/pnas.0510813103
52. Soh YQS, Junker JP, Gill ME *et al.* A gene regulatory program for meiotic prophase in the fetal ovary. *PLoS Genet* 2015;**11**:e1005531. https://doi.org/10.1371/journal.pgen.1005531
53. Schulz KN, Harrison MM. Mechanisms regulating zygotic genome activation. *Nat Rev Genet* 2019;**20**:221–34. https://doi.org/10.1038/s41576-018-0087-x
54. Seki Y, Yamaji M, Yabuta Y *et al.* Cellular dynamics associated with the genome-wide epigenetic reprogramming in migrating primordial germ cells in mice. *Development* 2007;**134**:2627–38. https://doi.org/10.1242/dev.005611
55. Bonnerot C, Vernet M, Grimber G *et al.* Transcriptional selectivity in early mouse embryos: a qualitative study. *Nucl Acids Res* 1991;**19**:7251–7. https://doi.org/10.1093/nar/19.25.7251
56. Sassone-Corsi P. Unique chromatin remodeling and transcriptional regulation in spermatogenesis. *Science* 2002;**296**:2176–8. https://doi.org/10.1126/science.1070963
57. Sanz LA, Kota SK, Feil R. Genome-wide DNA demethylation in mammals. *Genome Biol* 2010;**11**:110. https://doi.org/10.1186/gb-2010-11-3-110
58. Baudat F, Imai Y, de Massy B. Meiotic recombination in mammals: localization and regulation. *Nat Rev Genet* 2013;**14**:794–806. https://doi.org/10.1038/nrg3573
59. Hoghoughi N, Barral S, Vargas A *et al.* Histone variants: essential actors in male genome programming. *J Biochem* 2018;**163**:97–103. https://doi.org/10.1093/jb/mvx079
60. Huang Y, Li L, An G *et al.* Single-cell multi-omics sequencing of human spermatogenesis reveals a DNA demethylation event associated with male meiotic recombination. *Nat Cell Biol* 2023;**25**:1520–34. https://doi.org/10.1038/s41556-023-01232-7
61. Alexander AK, Rice EJ, Lujic J *et al.* A-MYB and BRDT-dependent RNA polymerase II pause release orchestrates transcriptional regulation in mammalian meiosis. *Nat Commun* 2023;**14**:1753. https://doi.org/10.1038/s41467-023-37408-w
62. Kaye EG, Basavaraju K, Nelson GM *et al.* RNA polymerase II pausing is essential during spermatogenesis for appropriate gene expression and completion of meiosis. *Nat Commun* 2024;**15**:848. https://doi.org/10.1038/s41467-024-45177-3
63. Braccioli L, de Wit E. CTCF: a Swiss-army knife for genome organization and transcription regulation. *Essays Biochem* 2019;**63**:157–65.
64. Yuen KC, Gerton JL. Taking cohesin and condensin in context. *PLoS Genet* 2018;**14**:e1007118. https://doi.org/10.1371/journal.pgen.1007118
65. Wang J, Bando M, Shirahige K *et al.* Large-scale multi-omics analysis suggests specific roles for intragenic cohesin in transcriptional regulation. *Nat Commun* 2022;**13**:3218. https://doi.org/10.1038/s41467-022-30792-9
66. Lengronne A, Katou Y, Mori S *et al.* Cohesin relocation from sites of chromosomal loading to places of convergent transcription. *Nature* 2004;**430**:573–8. https://doi.org/10.1038/nature02742
67. Borrie MS, Campor JS, Joshi H *et al.* Binding, sliding, and function of cohesin during transcriptional activation. *Proc Natl Acad Sci USA* 2017;**114**:E1062–71. https://doi.org/10.1073/pnas.1617309114
68. Khobta A, Epe B. Interactions between DNA damage, repair, and transcription. *Mutat Res* 2012;**736**:5–14. https://doi.org/10.1016/j.mrfmmm.2011.07.014
69. Slobodin B, Bahat A, Sehrawat U *et al.* Transcription dynamics regulate poly(A) tails and expression of the RNA degradation machinery to balance mRNA levels. *Mol Cell* 2020;**78**:434–44. https://doi.org/10.1016/j.molcel.2020.03.022
70. Lin Y, Gill ME, Koubova J *et al.* Germ cell-intrinsic and -extrinsic factors govern meiotic initiation in mouse embryos. *Science* 2008;**322**:1685–7. https://doi.org/10.1126/science.1166340
71. Harigaya Y, Tanaka H, Yamanaka S *et al.* Selective elimination of messenger RNA prevents an incidence of untimely meiosis. *Nature* 2006;**442**:45–50. https://doi.org/10.1038/nature04881
72. Kadyk LC, Kimble J. Genetic regulation of entry into meiosis in *Caenorhabditis elegans*. *Development* 1998;**125**:1803–13. https://doi.org/10.1242/dev.125.10.1803
73. Nousch M, Yeroslaviz A, Habermann B *et al.* The cytoplasmic poly(A) polymerases GLD-2 and GLD-4 promote general gene expression via distinct mechanisms. *Nucleic Acids Res* 2014;**42**:11622–33. https://doi.org/10.1093/nar/gku838

Received: May 5, 2024. **Revised:** February 6, 2025. **Editorial Decision:** February 9, 2025. **Accepted:** March 13, 2025